

## Octahedral Tilting in Perovskites. II. Structure Stabilizing Forces

PATRICK M. WOODWARD†

Department of Chemistry and Center for Advanced Materials Research, Oregon State University, Corvallis, OR 97331-4003, USA. E-mail: pat@pix7a.phy.bnl.gov

(Received 17 April 1996; accepted 28 August 1996)

### Abstract

The 23 Glazer tilt systems describing octahedral tilting in perovskites have been investigated. The various tilt systems have been compared in terms of their *A*-cation coordination and it is shown that those tilt systems in which all the *A*-cation sites remain crystallographically equivalent are strongly favored, when all the *A* sites are occupied by the same ion. Calculations based on both ionic and covalent models have been performed to compare the seven equivalent *A*-site tilt systems. Both methods predict that when the tilt angles become large, the orthorhombic  $a^+b^-b^-$  tilt system will result in the lowest energy structure. This tilt system gives the lowest energy structure because it maximizes the number of short *A*—O interactions. The rhombohedral  $a^-a^-a^-$  tilt system gives a structure with a slightly lower Madelung energy, but increased ion–ion repulsions destabilize this structure as the tilt angles increase. Consequently, it is stabilized by highly charged *A* cations and small to moderate tilt angles. The ideal cubic  $a^0a^0a^0$  tilt system is only observed when stabilized by oversized *A* cations and/or *M*—O  $\pi$ -bonding. Tilt systems with nonequivalent *A*-site environments are observed when at least two *A* cations with different sizes and/or bonding preferences are present. In these compounds the ratio of large-to-small cations dictates the most stable tilt system.

### 1. Introduction

The preceding article describes octahedral tilting distortions in the perovskite structure. In particular, the symmetry and crystallographic description of the 23 Glazer tilt systems are presented in detail. However, no suggestions are made as to the cause of these distortions. In this article the physical forces responsible for these tilts are discussed.

The fact that the vast majority of metallic ions in the periodic table can be incorporated into the perovskite structure makes it ideal for studying the role atomic properties (ionic radius, electronegativity, bonding preferences *etc.*) play in determining the structure and physical properties of crystalline materials. This fact

has long been realized by Goodenough who has written extensively on the magnetic (Goodenough, 1963) and electrical (Goodenough, 1971; Takano *et al.*, 1988) properties of perovskites. Goodenough and others have also compared different perovskite compounds in an attempt to understand the effects of bonding on the crystal structure and properties of solid-state materials (Goodenough, 1967; Choy, Park, Hong & Kim, 1994). Such work not only advances the scientific understanding of solid-state materials, but can also be a powerful tool for enhancing the physical properties of materials through structural modifications and atomic substitutions; one need only consider the vast body of synthetic research performed on the perovskite-related cuprates over the past decade to appreciate the importance of such understanding.

Although geometrical descriptions of the crystal systems describing octahedral tilting in perovskites and perovskite-like compounds have been treated comprehensively on several occasions (Glazer, 1972; Aleksandrov, 1976; Deblieck, Van Tendeloo, Van Landuyt & Amelinckx, 1985), a thorough and comprehensive treatment of the physical forces behind these distortions has never appeared in the literature. Despite the lack of a comprehensive treatment, several researchers have considered the structure-stabilizing forces associated with some of the more common tilt systems. Megaw & Darlington (1975) examined distortions in rhombohedral perovskites in detail, as did Thomas & Beitollahi (1994). The former study concluded that there were a variety of causes which led to distortion from ideal cubic symmetry, while the latter study showed that the tilt angle is strongly correlated with the polyhedral volume ratio of the *A* and *M* cations. Both studies also investigated octahedral distortions and *M*-cation shifts, which are not examined in this paper. In a later study, based once again on polyhedral volume ratio, Thomas compared the relative stabilities of cubic ( $a^0a^0a^0$ ), rhombohedral ( $a^-a^-a^-$ ) and orthorhombic ( $a^+b^-b^-$ ) perovskites. He concluded that the polyhedral volume of the *A* cation could be maximized, thereby reducing anion–anion repulsions, in the orthorhombic structure, explaining why this tilt system is so frequently observed when the *A* cation becomes small. Computational approaches using the concept of static energy surfaces have also been

† Current address: Department of Physics, Brookhaven National Laboratory, Upton, NY 11973, USA.

used to predict the temperatures of phase transitions between different tilt systems in halide-based perovskites (Flocken, Guenther, Hardy & Boyer 1985, 1986). This approach, although capable of giving accurate and detailed results for individual compounds, does not provide insight into the underlying cause of the distortion. Furthermore, the time and computational requirements associated with this method are prohibitive for everyday use by experimentalists. The research contained in this article seeks to go beyond earlier works in this field by considering all 23 Glazer tilt systems simultaneously, with the goal of understanding the factors stabilizing individual tilt systems.

## 2. A-cation coordination

Octahedral tilting causes the first coordination sphere about the *A* cation to change, in many cases, quite dramatically. At the same time, the first coordination sphere about the *M* cation is left virtually unchanged. Therefore, it is logical to assume that to a first approximation octahedral tilting is driven by the need to optimize the anion coordination about the *A* cation. This fact is widely accepted and was first pointed out almost 70 years ago by Goldschmidt. He calculated the optimal size of the *A* cation from ionic radii by treating the lattice as a close-packed array of hard spheres. If the combination of ions is the right size to close-pack perfectly, twice the *M*—*O* bond distance is equal to the cell edge and twice the *A*—*O* distance is equal to the length of a face diagonal. Goldschmidt first recognized this geometric relationship and quantified the quality-of-fit of the *A* cation with a factor known as the Goldschmidt tolerance factor, *t* (Goldschmidt, 1926)

$$t = (R_A + R_O) / [2^{1/2}(R_M + R_O)].$$

In the case of complex perovskites where more than one ion occupies the *M* and/or *A* sites, the average radius of the ions on each site is used for  $R_M$  and  $R_A$ , respectively. Compounds in the perovskite family are found to exist over the range  $1.05 > t > 0.78$  (Randall, Bhalla, Shrout & Cross, 1990).

Although the Goldschmidt tolerance factor can be useful for predicting whether a tilting distortion is expected, it does not directly give any information about which of the 23 tilt systems will be observed for a given combination of ions. To understand octahedral tilting on that level one must look carefully at the *A*-cation coordination from one tilt system to the next. The first step in understanding the effect of *A*-cation coordination is to systematically describe the *A*-cation coordination associated with each tilt system. In order to do this structures were generated by *POTATO* (Woodward, 1997) for ten different tilt systems and the *A*-cation coordination in each of these structures was examined. The tilt systems that were studied were the most

symmetric representatives of each of the ten classes of tilt systems: 000, 00–, 00+, 0++, 0+–, 0––, –––, +––, +–+ and ++++. The most symmetric tilt systems were chosen so that the tilt angles could remain constant from one system to the next. Analysis of less symmetric tilt systems would be difficult to carry out in a systematic way. For example, in the tilt system  $a^0b^-c^-$ , if the tilt angle about the *z* axis is taken to be 10°, what should the tilt angle about the *y* axis be? If that value is very small the *A*-cation coordination will be similar to that found in  $a^0a^0c^-$ , while if the tilting about *y* is near 10° the *A*-cation coordination will be similar to that found in  $a^0b^-b^-$ , and if the tilt angle is intermediate the coordination will be different still. Therefore, only the symmetric tilt systems are analyzed and the *A*-cation coordination spheres in the less symmetric tilt systems are assumed to be a modification of the coordination spheres found in the more symmetric tilt systems.

Table 1 summarizes the results of this study. This table was generated by starting with an *M*—*O* bond distance of 2.00 Å and setting all tilt angles to 10°. Some space groups allow the *A* cation to move off its ideal site, in those cases the *A* cation has been shifted in an attempt to give the most symmetric coordination geometry. The reduced coordination numbers of the *A* cation are a result of some of the anions moving too far away to be considered a significant part of the coordination sphere. Specifically, any anions more than 3.00 Å away from the *A* cation were considered to be outside the coordination sphere. The bond-valence calculations were performed by assuming the composition was SrTiO<sub>3</sub>. These numbers are only meaningful when compared relative to the other values found in Table 1. The bond-valence method, based on ideas originally put forward by Pauling (1929), was developed primarily by Brown (1981) and O'Keeffe (1989). This method assigns a valence to each bond in a crystal, based on the distance between ions. The calculations are empirical and make no assumption about the degree of ionicity/covalency in each bond. In a well behaved compound the bond valence of each ion will be close to its oxidation state (*i.e.* in SrTiO<sub>3</sub> the bond valences are expected to be Sr = +2, Ti = +4 and O = –2). The bond-valence calculations were performed with the program *Eutax* (O'Keeffe, 1992). The calculational details are described in more detail by Brese & O'Keeffe (1991).

One principle clearly illustrated in Table 1 is the fact that in some tilt systems all the *A*-cation sites remain crystallographically equivalent, while in other tilt systems the *A*-cation sites become nonequivalent. The *A*-cation coordination geometry in each of the six tilt systems with equivalent *A*-site positions is shown in Fig. 1. Fig. 1(a) shows the *A*-cation coordination for the ideal undistorted structure (tilt system 23). The *A* cation is coordinated by 12 equidistant anions in a cubo-octahedral geometry. This coordination can best be described by placing the *A* cation at the center of a cube

Table 1. *The A cation coordination in each of the ten tilt-system classifications*

This table was generated using *POTATO* with all tilt angles either 10 or 0° and a metal–oxygen distance of 2.00 Å. Bond-valence calculations were performed with the program *Eutax*, by assuming the compound was SrTiO<sub>3</sub>. The cell volumes have been normalized to the small perovskite cell containing one formula unit.

Tilt system	A-cation sites(s)	Coordination number	Bond distances (Å)	Geometry first coordination sphere	Bond valence	Cell volume (Å <sup>3</sup> )	Fig.
$a^0a^0a^0$ ( <i>Pm3m</i> )	(1b)	12	12 × 2.83	Cubo-octahedral	1.76	64.00	1(a)
$a^0a^0c^-$ ( <i>I4/mcm</i> )	(4b)	4 + 4	4 × 2.58 4 × 2.79	Distorted tetrahedral (Angles = 78 and 127°)	2.13	62.13	1(b)
$a^0a^0c^+$ ( <i>P4/mbm</i> )	(2c)	4 + 4	4 × 2.58 4 × 2.79	Rectangular planar (Angles = 78 and 102°)	2.13	62.13	1(c)
$a^0b^-b^-$ ( <i>Imma</i> )	(4e) (z = 0.72)	5 + 2	5 × 2.42–2.45 2 × 2.90	Square pyramidal	2.68	60.19	1(d)
$a^0b^+b$ ( <i>Cmcm</i> )	(4c) (y = 0.98)	4 + 2	4 × 2.39–2.41 2 × 2.74	Distorted tetrahedral (Angles = 84 and 123°)	2.71	60.20	None
	(4c)	6 + 2	6 × 2.53–2.56 2 × 2.83	Face-centered Trigonal prismatic	2.48		
$a^0b^+b^+$ ( <i>I4/mmm</i> )	(2a) (2b) (4c)	4 8 4 + 4	4 × 2.30 8 × 2.56 4 × 2.51	Square planar Square prismatic Rectangular planar	3.13 2.61 2.34	60.20	None
	(y = 0.5)		4 × 2.82	(Angles = 79 and 101°) Trigonal planar	3.36	58.34	1(e)
$a^-a^-a^-$ ( <i>R3c</i> )	(2a)	3 + 6	3 × 2.25 6 × 2.83				
$a^+a^-a^-$ ( <i>Pnma</i> )	(4c) (x = 0.945, z = 0.01)	4 + 4	4 × 2.31–2.45 4 × 2.58–2.70	Distorted tetrahedral (Angles 85 and 109°)	3.02	58.38	1(f)
$a^+a^+a^-$ ( <i>P4<sub>2</sub>/nmc</i> )	(2a) (2b) (4d) (z = 0.20)	4 + 4 4 + 4 6 + 4	4 × 2.26 4 × 2.83 4 × 2.30 4 × 2.83	Distorted tetrahedral (Angles 92 and 119°) Square planar	3.60 3.25	58.38	None
			6 × 2.43–2.55 4 × 2.81	Face-centered Trigonal prismatic	2.76		
$a^+a^+a^+$ ( <i>Im3</i> )	(2a) (6b)	12 4 + 4	12 × 2.74 4 × 2.25 4 × 2.82	Distorted cubo-octahedral (Angles = 62°) Square planar	2.21 3.53	58.38	None

and the anions at the middle of each of the 12 edges of the cube.

Fig. 1(b) shows the A-cation coordination in the  $a^0a^0c^-$  tilt system. Here the octahedra have tilted about the [001] axis in opposite senses (clockwise and counter-clockwise) in adjacent layers. This results in four short, four medium and four long A—O distances. Neglecting the four most distant anions gives the coordination description in Table 1 and shown in Fig. 1(b). The four closest anions surround the A cation in a very distorted tetrahedron and the four anions in the second coordination sphere surround the A cation in a square-planar geometry. The bond distance between the four closest anions and the A cation is dependent upon tilt angle, becoming smaller as the tilt angle increases. However, regardless of the tilt angle the first coordination sphere is always severely distorted from tetrahedral. In the cubic structure there are four 120° and two 90° bond angles making up the tetrahedron, while after a 10° tilt operation the bond angles become 127 and 78°.

Fig. 1(c) shows the A-cation coordination for the tilt system  $a^0a^0c^+$  (#21). The octahedra tilt about the [001] axes here as they did for  $a^0a^0c^-$ , but now they tilt in

the same sense in adjacent layers. The bond distances and bond valences given in Table 1 are the same for this system as they were for the  $a^0a^0c^-$  system, but the A-cation coordination is somewhat different. Now the first coordination sphere is rectangular planar instead of distorted tetrahedral. As the tilt angle increases, the four closest anions move closer to the A-cation (and to each other) and the bond angles continue to distort away from 90°.

Fig. 1(d) shows the coordination about the A cation for tilt system  $a^0b^-b^-$  (#20). This is the most symmetric of the two-tilt systems where now the octahedra have tilted about both the [010] and [001] axes. The coordination is seven-coordinate with the nearest five cations arranged in a square-pyramidal geometry. Unlike earlier tilt systems, in space group *Imma*, the A cation has one free parameter. This gives the A cation some freedom to adjust its position to obtain the optimal coordination. For the 10° tilts used in Table 1, the distance to the apex ion of the square pyramid, before shifting the A cation, was a very short 2.25 Å. To obtain a more symmetrical environment the A cation was shifted toward the base of the square pyramid.

The fifth tilt system,  $a^-a^-a^-$ , represented in Fig. 1(e), gives rise to a rhombohedrally distorted unit cell. This tilt system can also be described by a single tilt angle about one body diagonal (threefold axis) of the cubic cell (Megaw & Darlington, 1975; O'Keeffe & Hyde, 1977; Hyde & Andersson, 1988; Thomas & Beitollahi, 1994). Here the A cations are nine-coordinate, as indicated in Table 1 and shown in Fig. 1(e). The three closest anions form a perfect trigonal planar coordination in a plane perpendicular to the threefold axis, while the other six anions are arranged in a twisted trigonal prism about the A cation. The  $10^\circ$  tilts used to generate the numbers in Table 1 are larger than the tilt angles observed in actual compounds adopting this tilt system. For example, the structure of  $\text{LaAlO}_3$  can be generated using approximately  $3^\circ$  tilts about each axis and in  $\text{NdAlO}_3$  there are three short Nd—O distances of 2.39 Å and six longer Nd—O distances of 2.66 Å (Marezio,

Dernier & Remeika, 1972). Therefore, the numbers in Table 1 suggesting three very short distances are somewhat exaggerated.

Fig. 1(f) shows the A-cation coordination for the tilt system  $a^+a^-a^-$  (#11). Both this tilt system and the less symmetric  $a^+b^-b^-$  (#10) tilt system result in an orthorhombic unit cell (the commonly observed  $\text{GdFeO}_3$  structure) for simple perovskites and a monoclinic unit cell when cation ordering is present. Table 1 shows that the A cation is eight-coordinate with four shorter and four longer bonds, all of them spread over a range of distances. As was the case for  $a^-a^-a^-$ , there is only one crystallographic site for the A cation. In contrast to  $a^-a^-a^-$ , the A-cation position now has two free parameters ( $x$  and  $z$  in  $Pnma$ ). This is very important as it allows the A cation to shift to a more favorable coordination as the short A—O distances become too small. The coordination sphere of the four closest oxygens is a distorted tetrahedral geometry similar to that found in the  $a^0a^0c^-$  tilt system. However, here the tetrahedron is less distorted. For example, in  $\text{YAlO}_3$  the six O—Y—O angles defining the tetrahedron are 83.4, 88.2, 108.5, 108.5, 127.3 and  $127.3^\circ$  (Diehl & Brandt, 1975). This compares with six  $90^\circ$  angles in the cubic structure or two  $88^\circ$  and four  $128^\circ$  angles in the  $a^0a^0c^-$  tilt system. The overall coordination geometry about the A cation is a distorted archimedean antiprism (square antiprism) in the  $a^+a^-a^-$  tilt system. As with the tilt system  $a^0b^-b^-$  (20), the geometry is dependent upon the exact shift of the A cation.

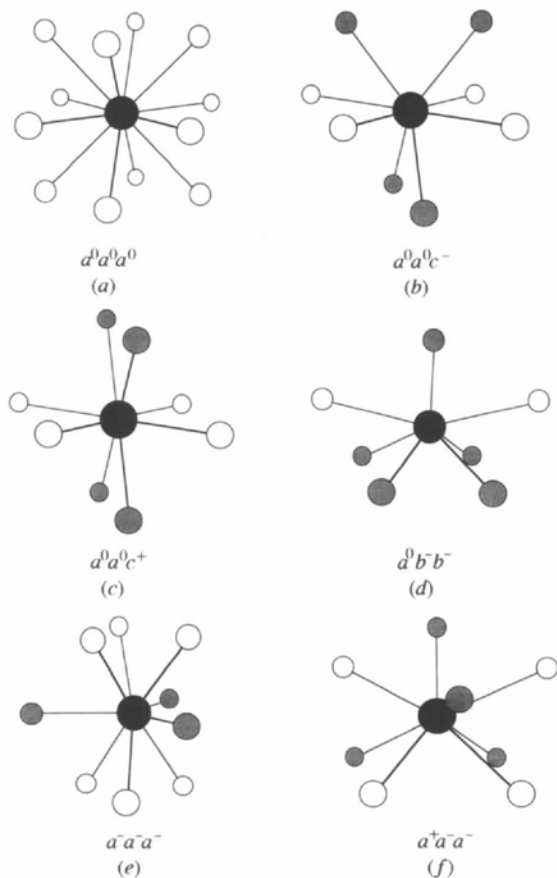


Fig. 1. The A-cation coordination for several of the tilt systems listed in Table 7. The different figures correspond to the A-cation coordination in (a)  $a^0a^0a^0$  (23), (b)  $a^0a^0c^-$  (22), (c)  $a^0a^0c^+$  (21), (d)  $a^0b^-b^-$  (20), (e)  $a^-a^-a^-$  (14) and (f)  $a^+a^-a^-$  (11). The filled circles represent the A cation, the lightly shaded circles the first anion coordination sphere and the open circles the second anion coordination sphere. The bond distances are as listed in Table 1.

### 3. Known tilt systems

In his original work Glazer (1972) gives known examples of tilt systems and he notes that only nine of the 23 tilt systems were found to exist among well characterized compounds at that time. Much work on both the synthesis and structural characterization of perovskites has been carried out since then, necessitating a search of the literature in order to update Glazer's list. The results of this search are given in Table 2, except for tilt systems  $a^+b^-b^-$  (10) and  $a^+a^-a^-$  (11), which are listed separately in Table 3. It is worth noting that since 1972 the scope of known compounds has expanded such that representatives of 15 of the 23 tilt systems are now known to exist. The total number of perovskite compounds is quite large, so despite the fact that the search was intended to be comprehensive, some omissions are inevitable. However, the focus of the search was to find compounds belonging to uncommon tilt systems, so that it is not likely that well characterized examples of the other eight tilt systems exist.

The  $a^+a^-a^-$  (11)/ $a^+b^-b^-$  (10) tilt systems are combined, because they both lead to structures with the same space group,  $Pnma$  (#62). Since there is no additional symmetry gained by keeping all three rotation angles equal, one might expect the  $a^+b^-b^-$  (10) tilt system to be

Table 2. *Examples of known tilt systems*

Tolerance factors have been calculated for the oxides and fluorides stable at room temperature and below, with unique or at least similar *A* cations. If no temperature is listed room temperature is implied. Covalent radii of Shannon have been used (Shannon, 1976). For the *A* cation 12-coordinate radii have been used, if necessary these radii have been extrapolated and two-coordinate anion radii have been used.

Tilt system	Tolerance factor	Compound	Reference
Three tilt systems		No known examples	
$a^+b^+c^+/a^+b^+b^+$		(Na <sub>0.25</sub> Mn <sub>0.75</sub> )MnO <sub>3</sub>	Marezio, Dernier, Chenevas & Joubert (1973)
		(Ca <sub>0.25</sub> Cu <sub>0.75</sub> )MnO <sub>3</sub>	Chenevas, Joubert, Marezio & Bochu (1975)
		(Ca <sub>0.25</sub> Cu <sub>0.75</sub> )TiO <sub>3</sub>	Bochu <i>et al.</i> (1979)
		(Tb <sub>0.17</sub> Cu <sub>0.75</sub> )TiO <sub>3</sub>	Bochu <i>et al.</i> (1979)
		(Na <sub>0.25</sub> Cu <sub>0.75</sub> )(Ta <sub>0.25</sub> Ti <sub>0.75</sub> )O <sub>3</sub>	Bochu <i>et al.</i> (1979)
		(Na <sub>0.25</sub> Cu <sub>0.75</sub> )(Nb <sub>0.25</sub> Ti <sub>0.75</sub> )O <sub>3</sub>	Bochu <i>et al.</i> (1979)
		(Na <sub>0.25</sub> Cu <sub>0.75</sub> )(Sb <sub>0.25</sub> Ti <sub>0.75</sub> )O <sub>3</sub>	Bochu <i>et al.</i> (1979)
		(Ca <sub>0.25</sub> Cu <sub>0.75</sub> )GeO <sub>3</sub>	Ozaki, Ghedira, Chenevas, Joubert & Marezio (1977)
		(Na <sub>0.25</sub> Cu <sub>0.75</sub> )RuO <sub>3</sub>	Labeau, Bochu, Joubert & Chenevas (1980)
		(Ca <sub>0.25</sub> Cu <sub>0.75</sub> )RuO <sub>3</sub>	Labeau, Bochu, Joubert & Chenevas (1980)
		(La <sub>0.25</sub> Cu <sub>0.75</sub> )RuO <sub>3</sub>	Labeau, Bochu, Joubert & Chenevas (1980)
		(Ca <sub>0.25</sub> Fe <sub>0.75</sub> )TiO <sub>3</sub>	Leinenweber & Parise (1995)
		(Th <sub>0.25</sub> Cu <sub>0.75</sub> )MnO <sub>3</sub>	Deschizeaux <i>et al.</i> (1976)
		(Y <sub>0.25</sub> Cu <sub>0.75</sub> )MnO <sub>3</sub>	Collomb, Samaras, Buevoz, Levy & Joubert (1983)
		(Nd <sub>0.25</sub> Cu <sub>0.75</sub> )RuO <sub>3</sub>	Müller, Haouzi, Laviron, Labeau & Joubert (1986)
		(Th <sub>0.25</sub> Cu <sub>0.75</sub> )MnO <sub>3</sub>	Fesenko, Razumovskaya, Shuvaeva, Gridneva & Bunina (1991)
		Li <sub>0.36</sub> WO <sub>3</sub>	Wiseman & Dickens (1976)
		Na <sub>0.73</sub> WO <sub>3</sub>	Wiseman & Dickens (1976)
		Na <sub>0.54</sub> WO <sub>3</sub>	Wiseman & Dickens (1976)
		D <sub>0.53</sub> WO <sub>3</sub>	Wiseman & Dickens (1973)
		D <sub>0.99</sub> MoO <sub>3</sub>	Parise, McCarron & Sleight (1987)
		HNbO <sub>3</sub>	Forquet <i>et al.</i> (1983)
$a^+b^+c^-$		NaNbO <sub>3</sub> (753–793 K)	Ahtee, Glazer & Megaw (1972)
$a^+a^+c^-$		CaFeTi <sub>2</sub> O <sub>6</sub>	Leinenweber & Parise (1995)
$a^+a^+c$		CaFeTi <sub>2</sub> O <sub>6</sub>	Leinenweber & Parise (1995)
$a^+b^+b^-/a^+a^+a^-$		No known examples	
$a^+b^-c^-/a^+a^-c^-$		WO <sub>3</sub> (~300–600 K)	Loopstra & Rietveld (1969)
		GaLiBr <sub>3</sub>	Hönle & Simon (1986)
		GaLiI <sub>3</sub>	Hönle, Miller & Simon (1988)
$a^-b^-c^-$		WO <sub>3</sub> (~230–300 K)	Diehl, Brandt & Salje (1978)
			Woodward, Sleight & Vogt (1995)
$a^-b^-b^-$		No known examples	
$a^-a^-a^-$	1.017	LaAlO <sub>3</sub>	Derighetti, Drumheller, Laves, Müller & Waldner (1965)
	1.014	LaCuO <sub>3</sub>	Demazeau, Parent, Pouchard & Hagenmueller (1972)
	1.011	LaCoO <sub>3</sub>	Thornton, Tofield & Hewat (1986)
	1.003	LaNiO <sub>3</sub>	García-Muñoz, Rodríguez-Carvajal, Lacorre & Torrance (1992)
	0.998	(Sr <sub>0.66</sub> La <sub>0.33</sub> )FeO <sub>3-x</sub>	Battle, Gibb & Lightfoot (1990)
	0.994	PrAlO <sub>3</sub> (298–205 K)	Burbank (1970)
	0.992	BaTbO <sub>3</sub>	Jacobson, Tofield & Fender (1972)
	0.991	(La <sub>0.75</sub> Sr <sub>0.25</sub> )CrO <sub>3</sub>	Khattak & Cox (1977)
	0.983	NdAlO <sub>3</sub>	Marezio, Dernier & Remeika (1972)
	0.974	NaNbO <sub>3</sub> (< 446 K)	Darlington (1971)
	0.960	BiFeO <sub>3</sub>	Michel, Moreau, Achenbach, Gerson & James (1969)
		HgTiO <sub>3</sub>	Sleight & Prewitt (1973)
		(Li <sub>0.66</sub> Cu <sub>0.33</sub> )TaO <sub>3</sub>	Sato, Jin, Hama & Uematsu (1993)
		(Sr <sub>1-x</sub> La <sub>x</sub> )FeO <sub>3</sub> (0.7 ≥ x ≥ 0.4)	Dann, Currie, Weller, Thomas & Al Rawwas (1994)
		PrNiO <sub>3</sub> (> 673 K)	Huang, Parrish, Toraya, Lacorre & Torrance (1990)
		LiNbO <sub>3</sub>	Megaw (1968)
		LiTaO <sub>3</sub>	Abrahams & Berstein (1967)
		MF <sub>3</sub>	Hepworth, Jack, Peacock & Westland (1957)
		<i>M</i> = Fe, Co, Ru, Rh, Pd, Ir	
Two-tilt systems		No known examples	
$a^0b^+c^+/a^0b^+b^+$		SrZrO <sub>3</sub> (973–1103 K)	Ahtee, Glazer & Hewat (1978)
$a^0b^+c^-/a^0b^+b^-$		NaNbO <sub>3</sub> (793–848 K)	Ahtee, Glazer & Megaw (1972)
		NaTaO <sub>3</sub> (803–873 K)	Ahtee & Darlington (1980)
		NH <sub>4</sub> MnCl <sub>3</sub> (128 K)	Tornero, Cano, Fayos & Martinez-Ripoll (1978)
$a^0b^-c^-$	0.994	PrAlO <sub>3</sub> (< 135 K)	Burbank (1970)

Table 2 (cont.)

Tilt system	Tolerance factor	Compound	Reference
$a^0b^-b^-$	0.985	BaPbO <sub>3</sub>	Marx <i>et al.</i> (1992) Ritter <i>et al.</i> (1989)
	0.997	Ba(Pb <sub>1-x</sub> Bi <sub>x</sub> )O <sub>3</sub> ( $0.2 \geq x \geq 0$ )	Marx <i>et al.</i> (1992)
	0.985	(Pr <sub>0.65</sub> Ba <sub>0.35</sub> )MnO <sub>3</sub> (298 K)	Jirak, Pollert, Andersen, Grenier & Hagenmuller (1990)
	0.994	BaPbO <sub>3</sub> (4 K)	Thornton & Jacobson (1976)
	0.994	PrAlO <sub>3</sub> (151–205 K)	Burbank (1970)
One-tilt systems		Ba(Pb <sub>1-x</sub> Bi <sub>x</sub> )O <sub>3</sub> ( $0.75 \geq x \geq 0.35$ )	Marx <i>et al.</i> (1992)
		Ba(Pb <sub>0.8</sub> Ti <sub>0.2</sub> )O <sub>2.8</sub>	Greedan, Willmer & Gibbs (1992)
$a^0a^0c^-$		NaTaO <sub>3</sub> (893 K)	Ahtee & Darlington (1980)
		NaNbO <sub>3</sub> (848–914 K)	Glazer & Megaw (1972)
$a^0a^0c^-$	1.009	CsSnI <sub>3</sub> (351–425 K)	Yamada <i>et al.</i> (1991)
	1.006	CsDyBr <sub>3</sub>	Hohnstedt & Meyer (1993)
	0.997	SrTiO <sub>3</sub> (< 110 K)	Unoki & Sakudo (1967)
	0.978	CsAgF <sub>3</sub>	Odenthal & Hoppe (1971)
	0.955	(Pr <sub>0.65</sub> Ba <sub>0.35</sub> )MnO <sub>3</sub> (210 K)	Jirak, Pollert, Andersen, Grenier & Hagenmuller (1990)
		KMnF <sub>3</sub> (88–184 K)	Minkiewicz, Fujii & Yamada (1970)
		RbAgF <sub>3</sub>	Odenthal & Hoppe (1971)
		SrZrO <sub>3</sub> (1103–1443 K)	Ahtee, Glazer & Hewat (1978)
Zero-tilt systems		WO <sub>3</sub> (740–953 K)	Salje (1977)
		Ba(Pb <sub>0.8</sub> Bi <sub>0.2</sub> )O <sub>3</sub> (453 K)	Marx <i>et al.</i> (1992)
$a^0a^0a^0$	1.049	SrGeO <sub>3</sub>	Shimizu, Syono & Akimoto (1970)
	1.047	BaMoO <sub>3</sub>	Brixner (1960)
	1.032	KMgF <sub>3</sub>	Zhao <i>et al.</i> (1996)
	1.031	BaNbO <sub>3</sub>	Svensson & Werner (1990)
	1.026	BaSnO <sub>3</sub>	Smith & Welch (1960)
	1.022	SrVO <sub>3</sub>	Rey <i>et al.</i> (1990)
	1.021	KZnF <sub>3</sub>	Buttner & Maslen (1988)
	1.020	SrFeO <sub>3</sub>	Takano <i>et al.</i> (1988)
	1.019	KCoF <sub>3</sub>	Kijima, Tanaka & Marumo (1981)
	1.014	KNiF <sub>3</sub>	Kijima, Tanaka & Marumo (1983)
	1.011	BaZrO <sub>3</sub>	Roth (1957)
	1.009	SrTiO <sub>3</sub>	Unoki & Sakudo (1967)
	1.002	KFeF <sub>3</sub>	Miyata, Tanaka & Marumo (1983)
	1.001	BaLiF <sub>3</sub>	Zhao <i>et al.</i> (1996)
	0.998	KUO <sub>3</sub>	Dickens & Powell (1991)
	0.986	SrMoO <sub>3</sub>	Liu, Zhao & Eick (1992)
	NaNbO <sub>3</sub> (> 914 K)	Glazer & Megaw (1972)	
	CsSnI <sub>3</sub> (> 426 K)	Yamada <i>et al.</i> (1991)	
	La <sub>0.14</sub> WO <sub>3</sub>	Wiseman & Dickens (1976)	
	ReO <sub>3</sub>	Ferretti, Rogers & Goodenough (1965)	

more commonly observed, because it has an additional degree of freedom. In an attempt to test this assertion, *POTATO* was used to simulate atomic positions of a handful of known structures. As expected, the  $a^+b^-b^-$  tilt system was found to be the correct tilt system in all cases. A somewhat unexpected result of these calculations was the observation that the two rotation angles tended to be very similar in magnitude, but in opposite directions (*i.e.* a clockwise rotation about the [100] axis and a counterclockwise rotation about the [010] and [001] axes).<sup>\*</sup> Why the rotations occur in opposite directions and how widely this generalization can be

extended remain unclear. All the calculational methods employed in this paper indicate no energetic difference between the two tilt systems (if the rotation magnitudes  $a$  and  $b$  are equal). Therefore, for the remainder of this paper the two tilt systems will be regarded as equivalent and will be referred to as the  $a^+b^-b^-$  (10) tilt system. A partial but extensive list of these compounds is given in Table 3.

Inspection of Tables 2 and 3 show that when the A site is occupied by a single type of cation the most commonly observed tilt systems are  $a^0a^0a^0$  (23),  $a^-a^-a^-$  (14) and  $a^+b^-b^-$  (10). From Table 1 one sees that all these tilt systems have crystallographically equivalent A-cation sites. In fact, at room temperature, all the compounds belonging to tilt systems with nonequivalent A sites have two different cations on the A site. This result is not

\* The direction of the tilts should not be confused with the phase of the tilts. Both  $a^+a^-a^-$  and  $a^+b^-b^-$  have in-phase tilting about the [100] axis and out-of-phase tilting about the [010] and [001] axes (see Fig. 1).

Table 3. *Examples of known  $a^+a^-a^-/a^+b^-b^-$  simple perovskites*

Tolerance factors have been calculated for those structures stable at room temperature and below. Covalent radii of Shannon have been used (Shannon, 1976). Tolerance factors have not been calculated for compounds with lone-pair *A* cations. If no temperature is listed it implies that the structural analysis was performed at room temperature.

Tilt system	Tolerance factor	Compound	Reference
$a^+b^-b^-$	1.012	CaMnO <sub>3</sub>	Poepfelmeier, Leonowicz, Scanlon, Longo & Yelon (1982)
$a^+a^-a^-$	1.012	CaGeO <sub>3</sub>	Sasaki, Prewitt & Liebermann (1983)
	1.001	SrRuO <sub>3</sub>	Jones, Battle, Lightfoot & Harrison (1989)
	0.986	CaVO <sub>3</sub>	Bouloux & Galy (1976)
	0.981	PrNiO <sub>3</sub> (571–673 K)	Lacorre <i>et al.</i> (1991)
	0.975	LaCrO <sub>3</sub>	Huang, Parrish, Toraya, Lacorre & Torrance (1990)
	0.974	NaTaO <sub>3</sub> (298–803 K)	Khattak & Cox (1977)
	0.974	NaTaO <sub>3</sub>	Ahtee & Darlington (1980)
	0.973	LaGaO <sub>3</sub>	Wang, Lu, Gao, Liberman & Dudley (1991)
	0.973	CaTiO <sub>3</sub>	Sasaki, Prewitt, Bass & Schulze (1987)
	0.972	SmAlO <sub>3</sub>	Koopmanns, van de Velde & Gellings (1983)
	0.967	SrSnO <sub>3</sub>	Marezio, Dernier & Remeika (1972)
	0.965	CaRuO <sub>3</sub>	Vegas, Vallet-Regi, Gonzales-Calbet & Alario-Franco (1986)
	0.964	KPdF <sub>3</sub>	Bensch, Schmalte & Reller (1990)
	0.962	CdTiO <sub>3</sub>	Alter (1974)
	0.961	LaMnO <sub>3</sub>	Sasaki, Prewitt, Bass & Schulze (1987)
	0.961	LaFeO <sub>3</sub>	Elemans, van Laar, van der Veen & Loopstra (1971)
	0.953	SrZrO <sub>3</sub> (973 K)	Geller & Wood (1956)
	0.951	DyAlO <sub>3</sub>	Ahtee, Glazer & Hewat (1978)
	0.951	CaMoO <sub>3</sub>	Ahtee, Ahtee, Glazer & Hewat (1976)
	0.951	BaPrO <sub>3</sub>	Bidaux & Mériel (1968)
	0.950	NdNiO <sub>3</sub>	Kamata, Nakamura & Sata (1975)
	0.947	BaPuO <sub>3</sub>	Jacobson, Tofield & Fender (1972)
	0.945	YAlO <sub>3</sub>	Lacorre <i>et al.</i> (1991)
	0.943	BaCeO <sub>3</sub>	Christoph <i>et al.</i> (1988)
	0.940	SmNiO <sub>3</sub>	Geller & Wood (1956)
	0.941	PrMnO <sub>3</sub>	Diehl & Brandt (1975)
	0.932	CaSnO <sub>3</sub>	Jacobson, Tofield & Fender (1972)
	0.930	KAgF <sub>3</sub>	Lacorre <i>et al.</i> (1991)
	0.928	SrPbO <sub>3</sub>	Quezel-Ambrunaz (1968)
	0.919	CaZrO <sub>3</sub>	Vegas, Vallet-Regi, Gonzales-Calbet & Alario-Franco (1986)
	0.918	NaUO <sub>3</sub>	Odenthal & Hoppe (1971)
	0.907	YCrO <sub>3</sub>	Keller, Meier & Müller-Buschbaum (1975)
	0.893	YFeO <sub>3</sub>	Koopmanns, van de Velde & Gellings (1983)
	0.889	SrCeO <sub>3</sub>	Bartram & Fryxell (1970)
	0.842	NaIO <sub>3</sub>	Geller & Wood (1956)
	0.96–	REVO <sub>3</sub>	Geller & Wood (1956)
	0.87	RE = La, Ce, Nd, Tb, Er, Tm, Yb	Saiki <i>et al.</i> (1991)
	0.95–	RETiO <sub>3</sub>	Svensson & Stahl (1988)
	0.88	RE = La, Nd, Sm, Gd, Y	Zubkov, Berger, Pesina, Bazuev & Shveikin (1986)
	0.94–	REFeO <sub>3</sub>	MacLean, Ng & Greedan (1979)
	0.88	RE = Pr–Lu	Marezio, Remeika & Dernier (1970)
	0.912	NaFeF <sub>3</sub>	Benner & Hoppe (1990)
	0.95–	NaMF <sub>3</sub>	Luetgert & Babel (1992)
	0.93	M = Ni, Mg, Cu, Zn, Co	
		MgSiO <sub>3</sub>	Hemley <i>et al.</i> (1989)
		SeMO <sub>3</sub>	Kohn, Inoue, Horie & Akimoto (1976)
		M = Mg, Mn, Co, Ni, Cu	
		TeMO <sub>3</sub>	Kohn, Inoue, Horie & Akimoto (1976)
		M = Mn, Co, Ni	
		BaUS <sub>3</sub>	Brochu, Padiou & Grandjean (1970)
		UCrS <sub>3</sub>	Noël, Padiou & Prigent (1975)
		YScS <sub>3</sub>	Rodier & Laruelle (1970)
		LaYbS <sub>3</sub>	Rodier, Julien & Tien (1983)
		KMgCl <sub>3</sub>	Brynstad, Yakel & Smith (1966)
		KMnCl <sub>3</sub>	Horowitz, Amit, Makovsky, Ben Dor & Kalman (1982)
		CsSnI <sub>3</sub>	Yamada <i>et al.</i> (1991)

surprising assuming the octahedra tilt in such a way as to optimize the coordination about the *A* cations. Assuming this is true, in cases where a single species occupies all the *A*-cation sites, one would expect the structure to distort in a manner that achieves the same optimal coordination about each *A* site. This principle was stated most eloquently almost 70 years ago by Linus Pauling as his fifth rule, the rule of parsimony (Pauling, 1929). The information in Tables 1 and 2 shows convincingly that for simple  $AMO_3$  compounds the rule of parsimony dictates that only tilt systems with equivalent *A* sites need be considered.

#### 4. Equivalent *A*-site tilt systems

It has been shown that there are seven tilt systems which lead to equivalent *A* sites;  $a^0a^0a^0$  (23),  $a^0a^0c^-$  (22),  $a^0a^0c^+$  (21),  $a^0b^-b^-$  (20),  $a^-a^-a^-$  (14),  $a^+a^-a^-$  (11) and  $a^+b^-b^-$  (10). However, Tables 2 and 3 show that there is not an even distribution of compounds among these tilt systems. By far the most commonly observed tilt system is  $a^+b^-b^-$  (10), followed by  $a^-a^-a^-$  (14) and  $a^0a^0a^0$  (23). This distribution of compounds raises some interesting questions. For example, what factors favor these three tilt systems over the others? For a given composition can we predict which tilt system will result? To answer these questions we need to understand what factors energetically favor the structure of one tilt system over the structures of competing tilt systems. To provide such an understanding both ionic and covalent bonding interactions must be considered. Both types of interactions must be examined because the bonding in perovskites is well known to be intermediate between the extremes of ionic and covalent bonding. Unfortunately, most comparative models are based primarily on either the ionic or the covalent model. Therefore, the seven equivalent *A*-site tilt systems have been analyzed using first an ionic model and then a covalent model. Hopefully, approaching the problem from both extremes will lead to an improved understanding of the intermediate regime.

##### 4.1. Ionic bonding

Ionic interactions in solids include both coulombic interactions and short-range noncoulombic interactions, such as Pauli repulsion and dispersion forces. Total lattice energy calculations using empirically derived atomic parameters provide one way of modeling these interactions (Bush *et al.*, 1992; Mackrodt, 1984). In these calculations each ion is typically modeled as a core and a shell. The ionic charge is empirically divided between the core and the shell and the force that holds the two together is approximated by a harmonic spring constant. Both the coulombic and noncoulombic interactions between the various cores and shells are then calculated, based on empirically derived potentials for

each ion. The core/shell approach allows the calculations to approximate the effect of polarization, particularly polarization of the oxygen electron cloud by highly charged cations. The key to performing meaningful calculations is to obtain a good set of empirical potentials for each ion in the structure. The empirical potentials for a given system are usually derived by fitting experimental data on the compound or compounds of interest. This approach, however, is of limited usefulness in comparing known structures with hypothetical structures, because the empirical potentials cannot help but show a bias in favor of the known structure from which they were derived. Fortunately, a self-consistent set of potentials was recently derived for oxides (Bush, Gale, Catlow & Battle, 1994). This set of transferable potentials was derived from binary oxides and allows this powerful calculational approach to be used as a predictive and a comparative tool for more complex oxide structures. All the calculations in this paper were performed with the General Utility Lattice Program (*GULP*), written by Julian Gale of Imperial College, London (Gale, 1992/1994).

The most significant structural change caused by octahedral tilting is the distortion of the *A*-cation coordination sphere. Given the large difference in electronegativity between typical *A* cations and oxygen, the bonding between the two species is expected to be largely ionic. Therefore, it seems reasonable to expect that calculations based on ionic energies may explain the observed distribution of structures. Using *POTATO* idealized structures can be easily generated in any of the 23 tilt systems. The lattice energies of these structures can then be compared using *GULP*. The difficulty lies in determining when structures from different tilt systems and space groups are equivalent. Obviously, by keeping the *M*—O bond distance constant the first coordination sphere about the *M* cation can remain unchanged from one tilt system to the next. Beyond that it becomes somewhat subjective as to what additional constraints to impose on each structure in order to define equivalency from one tilt system to the next. This problem is particularly apparent when attempting to compare structures from tilt systems with differing numbers of tilts (*i.e.* the three-tilt systems  $a^+b^-b^-$  and  $a^-a^-a^-$  with the two-tilt system  $a^0b^-b^-$ ). As this comparison is based primarily on an ionic model, the approach adopted in this analysis was to keep the unit-cell volume constant. In this way the calculations reveal the tilt system that can maximize ionic interactions within the same volume of free space.

$YAlO_3$  was chosen as the model compound for these calculations for a variety of reasons. First, to detect subtle differences in the *A*—O interactions it is best to use a compound that has a reasonably strong *A*—O interaction.  $YAlO_3$  is such a compound because of the relatively high oxidation state and electronegativity of yttrium (compared with other *A* cations such as  $Ba^{2+}$ ,  $Sr^{2+}$  and  $La^{3+}$ ). Secondly, the experimental octahedral

rotation angles are significant in this compound, which should also help to magnify the energetic differences between tilt systems. Finally, the  $\text{AlO}_6$  octahedra in this compound are very regular so that the assumption of perfect octahedra is a reasonably good one.

*POTATO* was used to generate the idealized structures that serve as the starting point for these calculations. The Al—O distance was taken to be 1.911 Å and the unit-cell volume of the  $2a_p \times 2a_p \times 2a_p$  unit cell was set equal to  $407.2 \text{ \AA}^3$ . Both these values were matched as closely as possible with the experimentally determined values from single-crystal structure solution (Diehl & Brandt, 1975). The rotation angles were as follows for each tilt system

$a^+b^-b^-(10)$	– 10.02, 10.02, 10.02°,
$a^-a^-a^-(14)$	10.00, 10.00, 10.00°,
$a^0b^-b^-(20)$	0, 12.23, 12.23°,
$a^0a^0c^+(21)$	0, 0, 17.29°,
$a^0a^0c^-(22)$	0, 0, 17.29°.

For the cubic system  $a^0a^0a^0(23)$ , in order to keep the volume at  $407.2 \text{ \AA}^3$ , the Al—O distance had to be shortened to 1.853 Å. Each structure was described as centrosymmetric triclinic, space group  $P\bar{1}$ , even though the true symmetry was always higher.

Using *GULP*, lattice energy calculations were performed on the starting structure associated with each tilt system. The ionic potentials used were taken directly from the set of transferable potentials mentioned earlier (Bush, Gale, Catlow & Battle, 1994). A Newton/Raphson minimization algorithm was employed. This allowed the program to stay in the local energy minimum associated with each tilt system. *GULP* is able to not only calculate the total lattice energy, but it also has the capability to vary certain structural parameters, under a variety of constraints, to minimize the energy. Using the minimization capabilities of *GULP* varying degrees of structural freedom were introduced in a stepwise fashion: first the *A*-site position was refined, the ion shells were refined, then all the ion positions were allowed to refine and finally the unit-cell constants were allowed to refine. The changes in energy were recorded after each step. The results of these calculations are plotted in Fig. 2. The lattice energy calculations on the initial structures show that the  $a^+b^-b^-$  tilt system (10) and the  $a^-a^-a^-$  tilt system (14) have the most favorable lattice energies, while the one- and zero-tilt system structures are less stable. The energies of the  $a^+b^-b^-$  and  $a^-a^-a^-$  systems are quite similar, but when the *Y* is allowed to shift off its ideal position, the energy of the  $a^+b^-b^-$  tilt system lowers by 0.056 eV, while the energy of the  $a^-a^-a^-$  tilt system remains unchanged. To illustrate why this should be, the *A*-cation environments in the  $a^+b^-b^-$ ,  $a^-a^-a^-$ ,  $a^0b^-b^-$  and  $a^0a^0a^0$  tilt systems are shown in Fig. 3. Notice that in the  $a^-a^-a^-$  system

the *A* cation sits on a threefold axis running along the [111] direction and a twofold axis running along the  $[1\bar{1}0]$  direction. The electric field gradient set up by the surrounding oxygen ions in this highly symmetrical environment make the ideal site for the *Y* ion a minimum on the potential energy surface. This keeps the *Y* ion from moving, despite the fact that the lattice energy minimizations were all carried out in space group  $P\bar{1}$ , so that no explicit symmetry constraints fix the *Y* ion to its ideal site. Turning now to the tilt system  $a^+b^-b^-$ , Fig. 3(a) shows that the *Y* ion sits on a mirror plane running perpendicular to the *x* axis. This restricts its movement in the *x* direction, but not in the *y* and *z* directions. The *Y* ion can then shift away from the three closest oxygens, shaded in black, and toward five of the six next-nearest oxygen ions, as indicated by the arrow in Fig. 3(a). This shifting of *Y* reduces the repulsion between yttrium and oxygen that arises when the octahedral tilting distortion becomes fairly large. Figs. 2 and 3(c) both show that *Y* can also shift in tilt system  $a^0b^-b^-$  (20), but the total energy of this tilt system is still higher than the  $a^+b^-b^-$  and  $a^-a^-a^-$  systems. This difference between the  $a^+b^-b^-$  and  $a^-a^-a^-$  tilt systems is crucial in stabilizing the  $a^+b^-b^-$  tilt system over the  $a^-a^-a^-$  tilt system as the tolerance factor decreases. The next stage in energy minimization was to let the ion shell positions refine, while keeping the ion cores stationary. Once again the energy of the  $a^+b^-b^-$  (10) structure decreases (becomes more stable), this time by 0.041 eV, while the energies of the  $a^-a^-a^-$  (14) and  $a^0b^-b^-$  (20) structures only increase by 0.015 and 0.005 eV, respectively. The decrease in energy during this stage of the refinement gives an estimate of how effectively the cation arrangement can

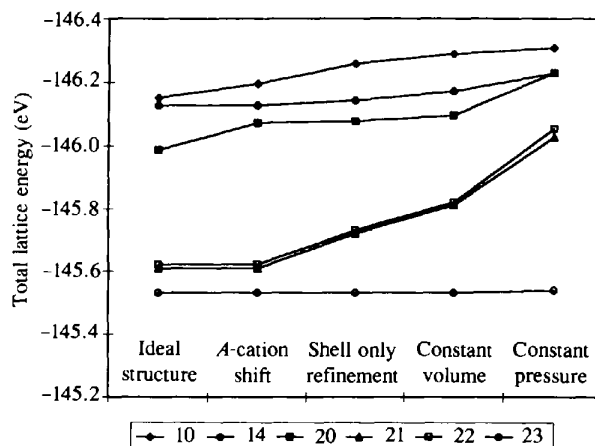


Fig. 2. Total lattice energy after each stage of the *GULP* refinements of the  $\text{YAlO}_3$  structure. Filled diamonds represent the  $a^+b^-b^-$  (10) tilt system, filled circles represent the  $a^-a^-a^-$  (14) tilt system, filled squares represent the  $a^0b^-b^-$  (20) tilt system, open triangles represent the  $a^0a^0c^+$  (21) tilt system, open squares represent the  $a^0a^0c^-$  (22) tilt system and open circles represent the  $a^0a^0a^0$  (23) tilt system.

polarize the electron clouds around the oxygen ions. One interesting observation was that if the shell refinement was performed before the Y ion was allowed to shift off its ideal site the decrease in energy in the  $a^+b^-b^-$  tilt system was only 0.011 eV. This is much lower than the 0.041 eV decrease observed if the shell refinement was carried out after shifting the Y ion, once again emphasizing the importance of the A-cation shift in the  $a^+b^-b^-$  tilt system.

The last two minimization steps in Fig. 2 are labeled constant volume and constant pressure. The former allows all the atom positions to refine, while the unit-cell constants remain fixed. The latter allows both the positional parameters and the unit-cell constants to refine simultaneously. The constant volume refinement removes the constraint that the octahedra must remain perfect. During this stage of the minimization the energy of the  $a^+b^-b^-$  tilt system decreases by 0.028 eV and the energy of the  $a^-a^-a^-$  tilt system decreases by 0.031 eV. The fact that both tilt systems show essentially the same decrease in energy implies that small distortions of the octahedra do not play a deciding role in determining the lowest energy structure. The constant pressure refinement removes the constraint that the unit-cell

volumes remain equal. When this constraint is removed the unit-cell volumes increase for all the structures (except the cubic  $a^0a^0a^0$  structure, which shows a slight decrease), which reduces both the coulombic attractions and the repulsive ion-ion interactions. Since the program minimizes the total energy, the benefit of reducing the repulsive terms will always outweigh the decrease in magnitude of the coulomb term. However, the final structure will be very dependent upon the empirical potentials used. For example, in the  $a^+b^-b^-$  tilt system the Y—O bond distances undergo relatively little change, but two of the six Al—O distances expand from 1.92 to 1.95 Å. This moves the structure away from the experimentally determined structure, yet only decreases the energy by a modest 0.019 eV. For this reason the constant volume minimization step seems to provide a more accurate comparison of the lattice energies of the different structures. The constant pressure minimization is included primarily to show that removing the constraint of constant volume does not change the overall conclusions reached earlier in the minimization process. Taking the refinement one step further the minimization algorithm can be changed from a Newton/Raphson to a rational function optimizer (r.f.o.) to avoid local minima. When this is done the final structure is always the orthorhombic  $a^+b^-b^-$  tilt system, regardless of the starting point, indicating that it is truly the global minimum in energy.

In order to quantitatively compare the results from the *GULP* calculations Table 4 contains the results obtained after the constant volume minimization stage. The trends in these results are representative of other points in the minimization process. The critical piece of information in this table is the fact that the rhombohedral  $a^-a^-a^-$  (14) tilt system maximizes the coulomb attraction between ions, but at the same time it also maximizes the repulsive energy term. In the case of  $\text{YAlO}_3$ , the repulsive term outweighs the attractive term and the  $a^+b^-b^-$  (10) tilt system gives the lowest energy structure. This trend was held throughout the minimization process and was also evident in calculations on other model compounds, such as  $\text{CaTiO}_3$  and  $\text{NdAlO}_3$ . The tilt system predicted by the calculations to have the lowest overall energy will be sensitive to the exact values of the empirical potentials employed. However, regardless of the empirical potentials employed, the conclusion that the  $a^-a^-a^-$  tilt system maximizes both the coulomb (Madelung) energy and the repulsive energy seems to be widely applicable. Both these properties are apparently a consequence of the high degree of symmetry found in this tilt system. Additional calculations show that the energy stabilization attributable to the coulomb term in the  $a^-a^-a^-$  system, with respect to the other tilt systems, decreases as the charge on the A cation decreases. This helps to explain why the rhombohedral distortion of the perovskite structure is commonly observed for  $A^{3+}M^{3+}O_3$  compounds, but rarely observed for  $A^{2+}M^{4+}O_3$  compounds.

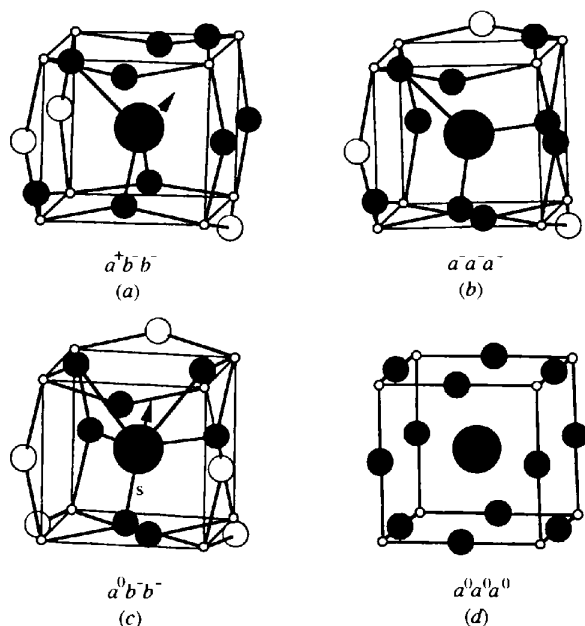


Fig. 3. The arrangement of oxygen ions about the A cation after octahedral tilting in  $\text{YAlO}_3$  in the (a)  $a^+b^-b^-$ , (b)  $a^-a^-a^-$ , (c)  $a^0b^-b^-$  and (d)  $a^0a^0a^0$  tilt systems. The large dark circles represent Y, the small open circles represent Al and the intermediate sized circles represent oxygen. The dark oxygens have the shortest Y—O distances, the shaded oxygens have intermediate Y—O distances and the open oxygens have the longest Y—O distances. In (c) the Y—O bond marked with an S is shorter than the other four short Y—O distances. The arrows in (a) and (c) indicate the direction in which the Y ion can shift in order to achieve a more even distribution of bond distances.

Table 4. *The results of total lattice energy (GULP) and bond-valence calculations on  $YAIO_3$  and idealized (constant volume)  $YAIO_3$  structures*

The cell volume was  $407.2 \text{ \AA}^3$  for each tilt system. Details of the calculation are given in the text.

	Total lattice energy (eV)	Repulsive energy (eV)	Attractive energy (eV)	Al—O—Al			
				Bond angles ( $^\circ$ )	Y	Al	O
Actual structure	-146.25	27.92	-174.17	151.7	3.16	2.97	2.14
$a^+b^-b^-$ (10)	-146.25	27.99	-174.24	151.9	3.19	2.97	2.10
$a^-a^-a^-$ (14)	-146.14	28.89	-175.03	151.8	3.39	2.97	2.03
$a^0b^-b^-$ (20)	-146.08	28.22	-174.29	151.9	3.26	2.97	2.12
$a^0a^0c^+$ (21)	-145.72	27.34	-173.06	145.4	3.01	2.97	2.06
$a^0a^0c^-$ (22)	-145.73	27.34	-173.07	180	3.01	2.97	2.06
$a^0a^0a^0$ (23)	-145.53	27.59	-173.12	180	1.87	2.97	1.61

Considering once again the tolerance factors of compounds in the various tilt systems, the overall trends can now be understood. Coulombic interactions favor the  $a^-a^-a^-$  (14) tilt system, when the repulsive interactions are relatively small. This is particularly true when the charge on the A cation is high and the tolerance factor is roughly in the range  $0.975 < t < 1.01$ . Repulsive interactions become important when the tolerance factor exceeds unity, because the oversized A cation is too large for the  $MO_3$  lattice. At this extreme the cubic  $a^0a^0a^0$  (23) tilt system is favored because it minimizes ion-ion repulsion. Repulsive interactions also become important when the tolerance factor becomes small ( $t < 0.975$ ), as shown above. In this situation the large rotation angles necessary to accommodate the undersized A cation lead to some rather short A—O distances, as well as increased anion-anion repulsions. In such cases the orthorhombic  $a^+b^-b^-$  (10) tilt system is favored, because it achieves the best balance between maximizing coulombic attractions and minimizing repulsive ion-ion interactions. This is due to the local symmetry about the A-cation site, which allows an A-cation shift and results in a better distribution of A—O distances. Thomas reached a similar conclusion when comparing orthorhombic and rhombohedral distortions of the perovskite structure (Thomas, 1996).

#### 4.2. Covalent bonding

The covalent bonding interactions of importance in perovskites are A—O  $\sigma$ -bonding, M—O  $\sigma$ -bonding and, when M is a transition metal, M—O  $\pi$ -bonding (Goodenough, 1971; Choy, Park, Hong & Kim, 1994; Takano *et al.*, 1991). Extended Hückel band structure

calculations using the tight binding approximation (EHTB) are one insightful way to evaluate bonding interactions in solids. These calculations have been used extensively to interpret and predict band structures of complex inorganic compounds (Hoffmann, 1988; Whangbo, Evain, Canadell & Ganne, 1989; Burdett & Mitchell, 1993). The extended Hückel method was developed initially by Hoffmann (1963) and later implemented on an extended solid by Whangbo & Hoffmann (1978). Hoffmann (1988) gives an excellent description of the interpretation and use of EHTB calculations in his book '*Solids and Surfaces*'. All extended Hückel tight binding (EHTB) calculations performed in this paper were carried out using the program *NEWS*, written by Dr Gordon Miller of Iowa State University (Miller, 1990). Default atomic parameters were used for all EHTB calculations in this work and are given in Appendix A. In the sections that follow EHTB calculations are used to examine more closely both A—O and M—O covalent bonding interactions.

4.2.1. *A—O bonding.* The same factors that made  $YAIO_3$  a good model compound for the ionic model lattice energy calculations make it a good model compound for examining A—O covalent bonding interactions. However, because of the strong dependence of covalent bond strength on exact bond distances, the constant volume approach for defining equivalent structures is not appropriate for a covalent model analysis. The problem once again is to define equivalent A-site environments from one tilt system to the next. One widely accepted and successful method of comparing ion-site environments across a variety of structures is the bond-valence concept (Brown, 1981; O'Keeffe, 1989). The bond valence and covalent bond strength of an ion are related in that they are both dependent upon the bond distances of the surrounding ions. The two concepts differ because the covalent bond interactions are also dependent upon the energetic and spatial overlap of atomic orbitals. Therefore, by keeping the ionic bond valences constant from one structure to the next, the average bonding capacity of each ion remains unchanged between structures. More sophisticated calculations, such as the extended Hückel method, can then differentiate the structures based on subtle geometrical differences in the ion coordination spheres of each structure. In other words, even though the average ion site environment is the same in all structures, small changes in the structure will modify orbital overlap and lead to varying degrees of covalent interactions. Using the bond-valence concept the following set of rules were used to generate equivalent structures:

(1) The M—O bond distance is set to a constant value, resulting in a constant bond valence for the M ion.

(2) For the  $a^+b^-b^-$  (10) tilt system the two rotation angles are constrained to be the same magnitude, but in opposite directions. For the other tilt systems studied,

Table 5. The results of extended Hückel, total lattice energy (*GULP*) and bond-valence calculations on  $YAlO_3$  and idealized  $YAlO_3$  structures

Only the ion shells were allowed to move in the *GULP* calculations. The bond valences of Y and Al were 3.164 and 2.971, respectively, for all systems, with the exception of  $a^0a^0a^0$  where the Y bond valence was 1.866. The details of the calculation are given in the text. Keep in mind that the energy differences are more important than the absolute values, especially for the extended Hückel calculations.

	Extended Hückel		Mulliken Y electron population	Total lattice energy (eV)	<i>GULP</i>		Al—O—Al bond angles (°)
	Total energy $YAlO_3$ (eV)	Total energy $AlO_3$ (eV)			Unit-cell volume (Å <sup>3</sup> )	Oxygen bond valence	
Actual structure	-471.31	-466.49	1.10	-146.23	203.6	2.136	151.7
$a^+b^-b^-$ (10)	-471.30	-466.50	1.10	-146.23	203.6	2.001	151.2
$a^-a^-a^-$ (14)	-471.14	-466.50	1.05	-146.20	205.8	2.139	152.0
$a^0b^-b^-$ (20)	-471.16	-466.52	1.06	-146.09	204.7	2.045	153.5
$a^0a^0c^+$ (21)	-470.98	-466.38	1.05	-145.62	201.2	2.136	146.4
$a^0a^0c^-$ (22)	-471.03	-466.38	1.07	-145.63	201.2	2.000	156.4
$a^0a^0a^0$ (23)	-469.54	-466.57	0.75	-145.27	223.3	1.892	180
						2.122	143.3
						1.892	180
						2.122	143.3
						1.613	180

such as  $a^-a^-a^-$  (14) and  $a^0b^-b^-$  (20), there are no ambiguities in the tilt angle relationships.

(3) The tilt angles are adjusted to give the same bond valence for the A cation, regardless of the structure (with the exception of the cubic structure where rule 1 completely determines the structure).

(4) If the A cation has free positional parameters they are adjusted to give bond-valence values for the oxygen ions that most closely match the bond-valence values found for the oxygen ions in the actual structure.

Using the above set of rules, equivalent structures were generated in tilt systems  $a^0a^0a^0$  (23),  $a^0a^0c^-$  (22),  $a^0a^0c^+$  (21),  $a^0b^-b^-$  (20),  $a^-a^-a^-$  (14) and  $a^+b^-b^-$  (10) for a hypothetical series of  $YAlO_3$  compounds. The bond valences of the ions were matched as closely as possible to the values found in the actual structure of  $YAlO_3$ : 3.16, 2.97, 2.14 and 2.00 for Y, Al, O1 and O2, respectively.

Extended Hückel calculations were carried out on the model  $YAlO_3$  structures. Table 5 shows the results of these calculations. The total energy of the valence electrons has been calculated for both  $YAlO_3$  and  $AlO_3^{3-}$  lattices in an attempt to separate effects due to Y—O bonding from those due to Al—O bonding. The total energy of the observed and idealized  $a^+b^-b^-$  structures are approximately the same, 0.15 eV lower than the  $a^0b^-b^-$  and  $a^-a^-a^-$  tilt systems, 0.30 eV lower than the one-tilt systems and 1.25 eV lower than the cubic structure. Table 5 also shows that if only Al—O bonding is considered, the lowest energy structure is the undistorted cubic structure. Its energy is slightly lower than the  $a^0b^-b^-$ ,  $a^-a^-a^-$  and  $a^+b^-b^-$  structures, which all have essentially the same energy. Lattice energy calculations, using *GULP*, were also performed on these structures

in order to compare ionic energies. The lattice energies become increasingly more favorable as the order of the tilt system increases. That is, the three tilt systems  $a^+b^-b^-$  and  $a^-a^-a^-$  have the lowest lattice energies and the zero-tilt system  $a^0a^0a^0$  has the highest lattice energy. The fact that the energy stabilization of the  $a^+b^-b^-$  tilt system disappears when either the Y atom is removed from the calculation or when ionic lattice energy calculations are performed implies that the energy stabilization of the  $a^+b^-b^-$  structure is directly attributable to covalent bonding interactions between yttrium and oxygen.

The calculation results in Table 5 indicate that the  $a^+b^-b^-$  tilt system leads to a structure that optimizes the bonding overlap between the A cation and oxygen. However, can an energy difference of 0.15 eV or 0.03% of the total energy be considered significant? Both experimental and theoretical calculations indicate that the magnitude of the energy difference between two competing structures can be as small as  $10^{-3}$ – $10^{-4}$  of the total lattice energy (Zunger, 1980). For example,  $BaTiO_3$  has a heat of formation of 152 kJ mol<sup>-1</sup> (Navrotsky, 1989). The lowest temperature phase transition in this material has a transformation heat of only 33 J mol<sup>-1</sup> (Galasso, 1969), or 0.02% of the heat of formation. The energy differences suggested by the EHTB calculations are of this order of magnitude. Nonetheless, one may still question if the way in which the idealized structures were generated was exact enough to warrant placing significance on such a small difference in energy. In order to check the sensitivity of the total EHTB energy to small changes in the bond-valence values the tilt angle of the  $a^-a^-a^-$  structure was changed so that the three closest A—O bond distances decreased by 0.01 Å each. Changing the structure in this way caused the bond

valence of Y to increase by 0.06, but the total EHTB energy changed only by 0.05 eV. If the Al—O distance was either shortened or lengthened by 0.01 Å (this also led to a changing of the nearest-neighbor Y—O distance of 0.01 Å), it caused the bond valence of Al to change by 0.08 and the bond valence of Y to change by 0.11. Despite the significant changes in both bond valences, the total EHTB energy change was relatively small, only 0.10 eV. On this scale the energy differences in Table 5 should be considered significant.

If Y—O bonding has a covalent component then the Y atomic orbitals must make a contribution to the density-of-states (DOS) below the Fermi level. Fig. 4 shows the DOS plots for several of the structures from Table 5. The shaded area is the partial density-of-states of the Y atom. Fig. 4 clearly indicates that Y makes a significant contribution to the DOS below the Fermi level. Furthermore, the DOS curves above the Fermi level change significantly from one tilt system to the next. The sensitivity of these levels to the Y coordi-

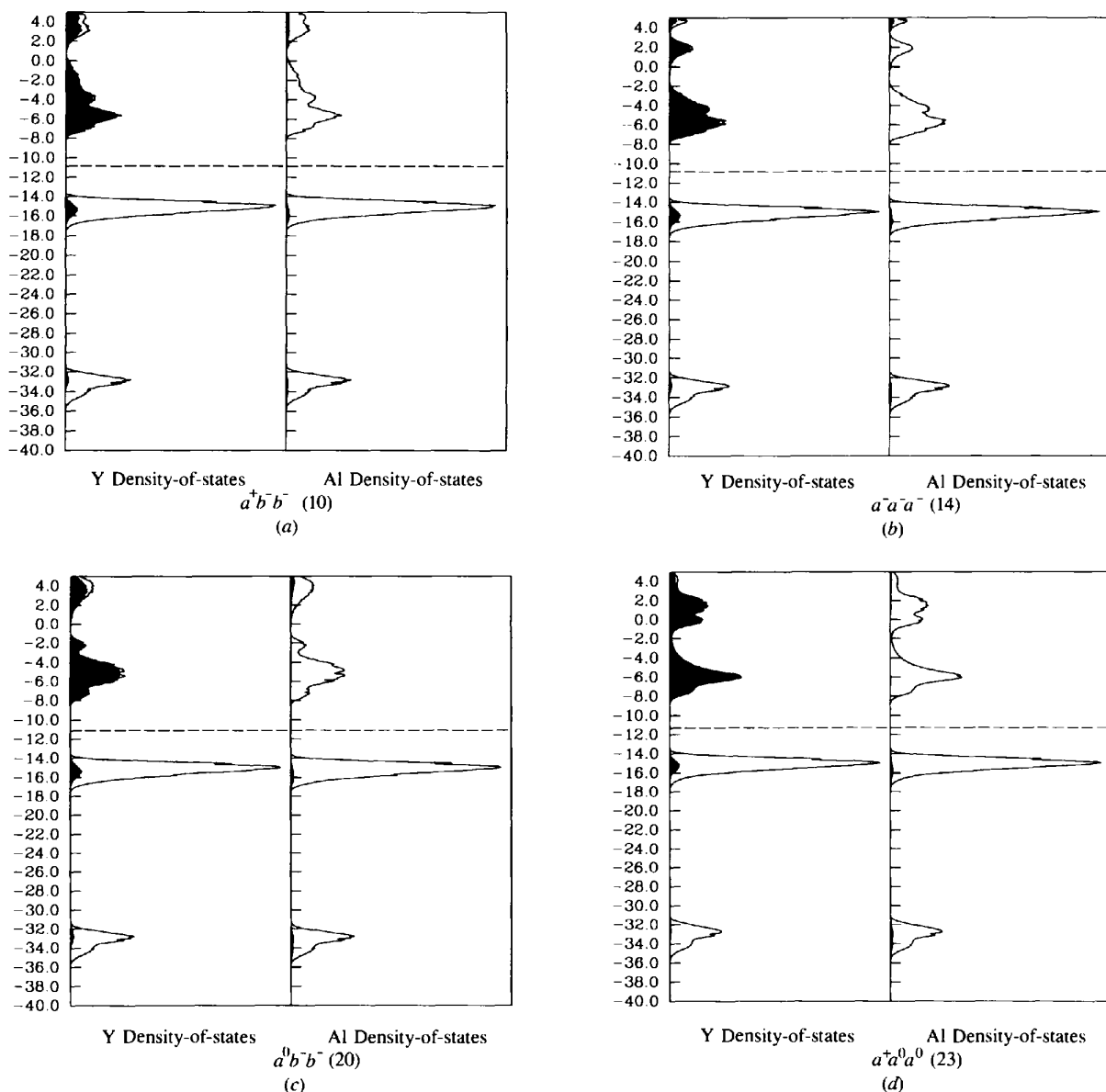


Fig. 4. Density-of-states plots for extended Hückel calculations on  $\text{YAlO}_3$ . The darkened curves on the left-hand side of each frame show the partial density of states contribution of Y, the darkened curves on the right-hand side of each frame show the partial density-of-states contribution of Al. DOS plots correspond to the following structures: (a)  $a^+ b^- b^-$ , (b)  $a^- a^- a^-$ , (c)  $a^0 b^- b^-$  and (d)  $a^0 a^0 a^0$  tilt systems.

nation is an indication that they are better described as antibonding rather than nonbonding. This conclusion is verified by the electron population values for Y, tabulated in Table 5. These values were calculated using the Mulliken population analysis method. This approach assigns all unshared electron density to the atoms from which the respective atomic orbitals originate and then equally divides the shared electron density between the neighboring atoms involved in bond overlap (Hoffmann, 1988). This approach is one arbitrary method of dividing up the electron density in the unit cell among the constituent atoms. Yttrium is not expected to possess any unshared (nonbonded) electrons so that all the electron density associated with yttrium in the Mulliken population analysis originates from Y—O bonding overlap. Table 5 shows Y population values on average just over 1 electron per yttrium, indicative of Y—O bond formation. In comparison, the Al ions are calculated to have electron population values in the range 1.02–1.06. Also note that tilt system  $a^+b^-b^-$  (10) shows the maximum electron density on the Y ion, suggesting it also has the maximum Y—O bonding overlap. This is consistent with the total energy values.

How can we understand the results of these calculations? What geometrical factor leads to the optimal A—O orbital overlap in the  $a^+b^-b^-$  tilt system? Two factors must be considered: the bond distances and symmetry of the anions about the A site. Considering first the symmetry, Fig. 1 clearly shows that in tilt systems  $a^-a^-a^-$  (14) and  $a^0a^0c^+$  (21) the first coordination sphere of oxygens about the A cation are coplanar. If the  $p_x$ - and  $p_y$ -orbitals of the A cation are directed in this plane, then the  $p_z$ - and the  $d_{z^2}$ -orbitals will both be orthogonal to this plane and will have zero overlap with the first coordination sphere of oxygens. In the corresponding tilt systems  $a^+b^-b^-$  (10) and  $a^0a^0c^-$  (22) the first coordination sphere of oxygens is no longer planar, increasing the number of A-cation orbitals that can participate in bonding. The distribution of bond distances also affects the orbital overlap, between yttrium and oxygen. Table 6 shows the bond distances, bond valences and crystal orbital overlap populations (COOP) for all 12 Y—O interactions in each tilt system. The majority of the Y—O bonding is confined to three oxygens in  $a^-a^-a^-$ , four oxygens in  $a^0a^0c^+$  and  $a^0a^0c^-$ , and five oxygens in the  $a^0b^-b^-$  system. In the  $a^+b^-b^-$  system bond-valence calculations suggest that eight oxygens effectively coordinate yttrium, while a crystal orbital overlap population (COOP) analysis performed in the EHTB calculations (Hoffmann, 1988) indicates a coordination number six. The yttrium coordination number six is supported by crystallographic data. In the rare earth orthoferrites  $AFeO_3$  the six closest A—O bond distances linearly decrease as the size of the rare earth ion decreases across the entire lanthanide series. In contrast, the seventh and eighth oxygen neighbors move slightly closer to the rare earth ion with decreasing size

Table 6. Y—O bond distances, bond valences and integrated COOP values for  $YAlO_3$  and idealized  $YAlO_3$  structures used in the EHTB analysis of  $YAlO_3$

The bond valences of the ions were matched as closely as possible to the values found in the actual structure of  $YAlO_3$ : 3.16, 2.97, 2.14 and 2.00 for Y, Al, O1 and O2, respectively.

	Y—O bond distances (Å)	Y—O bond valences	Y—O integrated COOP values
Actual structure	2.2370	0.5474	0.2126
	$2 \times 2.2843$	$2 \times 0.4817$	$2 \times 0.1933$
	2.3061	0.4541	0.1512
	$2 \times 2.4807$	$2 \times 0.2833$	$2 \times 0.1277$
	$2 \times 2.5691$	$2 \times 0.2230$	$2 \times 0.0601$
	3.0102	0.0677	0.0021
	3.1188	0.0505	0.000
$a^+b^-b^-$ (10)	$2 \times 3.2604$	$2 \times 0.0344$	$2 \times 0.000$
	2.1829	0.6335	0.2373
	$2 \times 2.2969$	$2 \times 0.4655$	$2 \times 0.1880$
	2.3597	0.3929	0.1311
	$2 \times 2.4682$	$2 \times 0.2930$	$2 \times 0.1340$
	$2 \times 2.5872$	$2 \times 0.2124$	$2 \times 0.0562$
	3.0290	0.0644	0.0041
	3.0670	0.0581	0.000
$a^+a^-a^-$ (11)	$2 \times 3.2513$	$2 \times 0.0353$	$2 \times 0.000$
	2.1893	0.6226	0.2341
	$2 \times 2.2906$	$2 \times 0.4735$	$2 \times 0.1905$
	2.3537	0.3993	0.1331
	$2 \times 2.4804$	$2 \times 0.2835$	$2 \times 0.1285$
	$2 \times 2.5782$	$2 \times 0.2176$	$2 \times 0.0581$
	3.0219	0.0656	0.0038
	3.0647	0.0584	0.000
$a^-a^-a^-$ (14)	$2 \times 3.2574$	$2 \times 0.0347$	$2 \times 0.000$
	$3 \times 2.1570$	$3 \times 0.6794$	$3 \times 0.3295$
	$6 \times 2.7026$	$6 \times 0.1555$	$6 \times 0.0328$
	$3 \times 3.0318$	$3 \times 0.0639$	$3 \times 0.000$
$a^0b^-b^-$ (20)	2.0825	0.8309	0.1909
	$4 \times 2.3354$	$4 \times 0.4195$	$4 \times 0.1867$
	$2 \times 2.7680$	$2 \times 0.1303$	$2 \times 0.0351$
	$4 \times 2.9241$	$4 \times 0.0854$	$4 \times 0.0060$
	3.0928	0.0542	0.000
$a^0a^0c^+$ (21)	$4 \times 2.2635$	$4 \times 0.5095$	$4 \times 0.1512$
	$4 \times 2.5654$	$4 \times 0.2253$	$4 \times 0.0801$
	$4 \times 3.0796$	$4 \times 0.5061$	$4 \times 0.000$
$a^0a^0c^-$ (22)	$4 \times 2.2635$	$4 \times 0.5095$	$4 \times 0.1559$
	$4 \times 2.5654$	$4 \times 0.2253$	$4 \times 0.0688$
	$4 \times 3.0796$	$4 \times 0.5061$	$4 \times 0.000$
$a^0a^0a^0$ (23)	$12 \times 2.7026$	$12 \times 0.1555$	$12 \times 0.0505$

only from La to Tb, then as the size of the rare earth ion decreases further these two A—O distances actually begin to increase (Marezio, Remeika & Dernier, 1970). The rare earth titanates,  $ATiO_3$ , also behave in a similar way (MacLean, Ng & Greedan, 1979). Regardless of whether the A-cation coordination is eight or six, the  $a^+b^-b^-$  system maximizes the coordination number of yttrium, as well as the number of orbitals on yttrium that can participate in Y—O bonding. Both these factors should help to make the  $a^+b^-b^-$  tilt system the most favorable in terms of A—O covalent bonding overlap.

How applicable are the  $YAlO_3$  results to other compounds? Obviously, as the electronegativity of the A cation increases, the importance of the covalent A—O

bonding interactions will increase and the  $a^+b^-b^-$  tilt system will become increasingly stable. The  $A-O$  bonding interactions will also play a more prominent role as the distortion from the cubic structure increases, due to the increased overlap of oxygen orbitals with the  $A$ -cation orbitals. For many of the basic cations found on the  $A$  site, the ionic arguments of Madelung energy and ion repulsion are probably the structure determining forces. One case in which the ionic arguments fail to predict the symmetry correctly is when  $A=Ca$ . When the  $A$  cation is  $Ca$  the orthorhombic  $GdFeO_3$  structure is almost always formed even when the tolerance factor is greater than one, as is the case for  $CaMnO_3$  (Poeppelmeier, Leonowicz, Scanlon, Longo & Yelon, 1982) and  $CaGeO_3$  (Sasaki, Prewitt & Liebermann, 1983). In these compounds presumably the orthorhombic, cubic and rhombohedral structures are all in competition. If ion core repulsion is the most important factor the cubic structure will be formed. If Madelung energy is the structure determining force, the rhombohedral structure will result and if  $A-O$  covalent bonding interactions outweigh Madelung energy and ion core repulsion, the orthorhombic ( $a^+b^-b^-$ ) structure will be the most stable. The fact that  $CaM^{4+}O_3$  compounds adopt the orthorhombic  $GdFeO_3$  structure, rather than the rhombohedral or cubic structures, would seem to indicate that there is a significant amount of covalency in the  $Ca-O$  bonds. Goodenough has long supported this point of view based on the physical properties of perovskite compounds (Goodenough, 1971; Takano *et al.*, 1991).

**4.2.2.  $M-O$  bonding.** No treatment of structure stabilizing forces in perovskites would be complete without considering covalent  $M-O$  interactions. With few exceptions, the  $M$  cation is more electronegative than the  $A$  cation. Consequently, the  $M-O$  interactions are expected to be stronger than the  $A-O$  interactions. The dominance of the  $M-O$  interactions is clearly demonstrated by the structural changes associated with octahedral tilting distortions. The coordination sphere about the  $A$  cation changes considerably, while the coordination sphere about the  $M$  cation remains, to a first approximation, unchanged. However, since the first coordination sphere about the  $M$  cation is the same in all tilt systems, one could argue that the  $M-O$  interactions have little influence in determining the lowest energy tilt system. Nonetheless, because of their strength they must be considered.

From the physical properties of perovskites it is well known that both  $M-O$   $\sigma$ - and  $M-O$   $\pi$ -bonding can play important roles (Goodenough, 1971). Since the  $M-O$  distances and octahedral coordination sphere are essentially the same in all 23 tilt systems, the major difference between structures will be the  $M-O-M$  angles (Marezio, Remeika & Dernier, 1970). As these angles distort from  $180^\circ$  the orbital overlaps that determine the strength of both the  $\sigma$ - and  $\pi$ -interactions will decrease.

In order to investigate the sensitivity of each of these two bonding interactions to changes in the  $M-O-M$  angles, extended Hückel calculations were performed on ideal  $MoO_3^{2-}$  and  $SnO_3^{2-}$  lattices. These two compounds were chosen because both  $Mo$  and  $Sn$  are tetravalent, belong to the same period of the periodic table and have similar ionic radii. The major difference between the two metal ions is the presence of partially filled  $d$ -orbitals on  $Mo^{4+}$ , which allow the formation of  $\pi$ - and  $\pi^*$ -bands in  $MoO_3^{2-}$ . Therefore, the  $MoO_3^{2-}$  energy will be sensitive to changes in both  $\sigma$ - and  $\pi$ -bonding overlaps, while the  $SnO_3^{2-}$  energy will only depend upon the  $\sigma$ -orbital overlap. Fig. 5 shows the results of these calculations. The electronic energy, as calculated by the extended Hückel method, is plotted against the magnitude of the rotation angles. The tilt system  $a^+b^-b^-$ , with perfect octahedra, was used for the analysis. The  $Mo-O$  and  $Sn-O$  distances were calculated from the standard ionic radii (Shannon, 1976). The energy of the  $MoO_3^{2-}$  lattice drops off twice as fast as the energy of the  $SnO_3^{2-}$  lattice. This suggests that both the  $\sigma$ - and  $\pi$ -covalent  $M-O$  interactions decrease at approximately the same rate as the  $M-O-M$  angle decreases.

When considering the effect of  $M-O$  bonding on determining the lowest energy tilt system, it is useful to consider  $AMO_3$  compounds where  $M$  is a  $p$ -block element separately from those compounds where  $M$  is a transition metal. When  $M$  is a  $p$ -block element,  $\pi$ -bonding does not contribute to the stability of the structure because the  $(n-1)d$ -orbitals are completely filled and the  $nd$ -orbitals are too high in energy to overlap significantly with the oxygen  $2p$ -orbitals. Even in the absence of  $\pi$ -bonding, the analysis up to this point still suggests that the cubic structure maximizes orbital overlap and hence  $M-O$  covalent bonding. However, as seen in Fig. 5 the energy destabilization due to decreased  $M-O$   $\sigma$ -bond overlap is relatively small for moderate tilt angles. This term may be overcome by gains in either ionic energy or the  $A-O$  covalency,

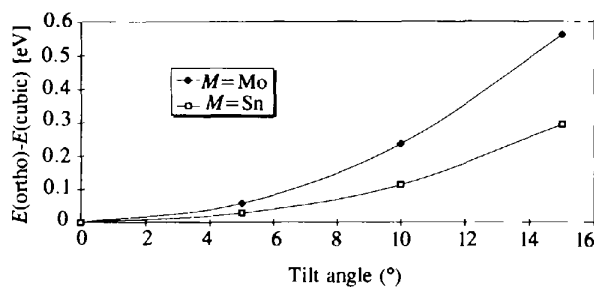


Fig. 5. The energy difference as calculated by the EHTB method between the cubic  $a^0a^0a^0$  tilt system and the orthorhombic  $a^+b^-b^-$  tilt system. The open squares represent calculations carried out on a  $SnO_3^{2-}$  lattice, where only  $M-O$   $\sigma$ -interactions are possible, and the filled diamonds represent calculations carried out on a  $MoO_3^{2-}$  lattice, where both  $\sigma$ - and  $\pi$ -interactions can contribute to the bonding.

both of which stabilize the distorted structures with respect to the cubic structure. Examining Tables 2 and 3 the only cubic perovskites that contain a  $p$ -block element as the  $M$  cation are  $\text{SrGeO}_3$  (Shimizu, Syono & Akimoto, 1970) and  $\text{BaSnO}_3$  (Smith & Welch, 1960). Both these compounds have tolerance factors (1.049 and 1.026, respectively) in the range where ion-ion repulsion strongly favors the cubic structure.  $\text{CaGeO}_3$  (Sasaki, Prewitt & Liebermann, 1983) and  $\text{LaAlO}_3$  (Derighetti, Drumheller, Laves, Müller & Waldner, 1965; de Rango, Tsoucarus & Zelwer, 1966) both have tolerance factors greater than unity, but both are distorted from cubic. Based on the behavior of these compounds it would appear as though  $M\text{—O}$   $\sigma$ -bonding, in the absence of  $M\text{—O}$   $\pi$ -bonding, does not play a major role in determining the lowest energy tilt system.

Simple geometry and the EHTB calculations on the  $\text{SnO}_3^{2-}$  lattice show that a  $180^\circ M\text{—O—}M$  bond angle leads to the maximum overlap between  $\sigma$ -orbitals on the octahedral cation and oxygen. However, the behavior of real compounds suggests that the cubic structure may not always lead to the maximum  $M\text{—O}$   $\sigma$ -bonding. Two examples which illustrate this point are  $\text{WO}_3$  and  $\text{NaSbO}_3$ . The  $\text{WO}_3$  structure has the same  $\text{MO}_3$  corner-sharing octahedral framework as the perovskite structure, but in  $\text{WO}_3$  the  $A$  cations are absent. From the simple overlap analysis given thus far one would expect  $\text{WO}_3$  to have a cubic structure. In fact, even though  $\text{WO}_3$  undergoes at least four phase transitions between 0 and 950 K, an octahedral tilting distortion is always present, along with a displacement of the tungstens from the center of the octahedra (Salje, 1977; Diehl, Brandt & Salje, 1978; Woodward, Sleight & Vogt, 1995). In this compound no  $A\text{—O}$  interactions are present, therefore,  $M\text{—O}$  bonding forces must be responsible for the observed distortions from cubic symmetry.  $\text{NaSbO}_3$  adopts the ilmenite structure with  $90^\circ M\text{—O—}M$  bond angles rather than the perovskite structure, even though the tolerance factor ( $t=0.994$ ) is almost ideal for the perovskite structure and the Madelung energy of the perovskite structure is more favorable. Since the  $\text{Na—O}$  bond is expected to be almost completely ionic, the ilmenite structure can only be stabilized by  $\text{Sb—O}$  covalency. Goodenough & Kafalas (1972) explain the behavior of this compound by pointing out that in a  $180^\circ \text{Sb—O—Sb}$  bond, only one oxygen  $p\sigma$ -orbital is present and it must simultaneously bond to both neighboring antimony ions. On the other hand, if the  $\text{Sb—O—Sb}$  bond angle is  $90^\circ$  then two of the  $p$ -orbitals on oxygen can participate in  $\sigma$ -bonding, each one to a separate antimony ion. For this reason the  $90^\circ \text{Sb—O—Sb}$  bond angle is expected to optimize the  $\text{Sb—O}$  covalent interaction.

Fig. 5 shows that the energy stabilization of the cubic structure, due to  $M\text{—O}$  covalency, is enhanced considerably when  $M\text{—O}$   $\pi$ -bonding can take place. Experimental evidence also suggests that  $M\text{—O}$   $\pi$ -

bonding can play an important role in stabilizing  $180^\circ$  bond angles. For example, both  $\text{NaNbO}_3$  and  $\text{NaTaO}_3$  crystallize in the orthorhombically distorted perovskite structure. This is in contrast to  $\text{NaSbO}_3$ , despite the fact that  $\text{Nb}^{5+}$  and  $\text{Ta}^{5+}$  have the same oxidation state and are almost the same size as  $\text{Sb}^{5+}$ . The structural change is thought to be driven by the overlap of the  $4d/5d$ -metal  $t_{2g}$ -orbitals with the oxygen  $p\pi$ -orbitals (Goodenough & Kafalas, 1972; Blasse, 1965). This overlap presumably drives the  $M\text{—O—}M$  angles much closer to the  $180^\circ$  value that maximizes  $\pi$ -bonding overlap. The importance of  $\pi$ -bonding as a structure-determining force can also be seen if the tungsten ions in  $\text{WO}_3$  are replaced with rhenium ions, to give  $\text{ReO}_3$ . The extra electron on rhenium partially fills the antibonding  $\pi^*$ -conduction band and leads to metallic conduction. At the same time the cubic structure is stabilized (Ferretti, Rogers & Goodenough, 1965; Morin, 1961). The same result can be obtained by introducing sodium ions, which donate their electrons to the  $\pi^*$ -band, onto the vacant  $A$ -cation site.  $\text{Na}_x\text{WO}_3$  is known to be metallic and cubic for  $0.32 \leq x \leq 0.93$  (Hägg, 1935). The fact that  $\text{ReO}_3$  is cubic while  $\text{WO}_3$ ,  $\text{NaNbO}_3$  and  $\text{NaTaO}_3$  all display octahedral tilting distortions suggests that not only the presence but the filling of the  $\pi$ - and  $\pi^*$ -bands will play a role in determining the structure.

Table 7 shows all the well characterized  $\text{AMO}_3$  perovskites where  $M$  is a transition metal ion and the tolerance factor is larger than 0.98. In those compounds with tolerance factors less than 0.98 the increase in ionic energy associated with the orthorhombic distortion ( $a^+b^-b^-$ ) seems to outweigh any  $M\text{—O}$   $\pi$ -bonding stabilization of the cubic structure. The majority of known cubic  $\text{AMO}_3$  perovskites are found in Table 7. The cubic structure is even found in some compounds, such as  $\text{SrMoO}_3$ , where the tolerance factor is less than one. This relatively high rate of occurrence of the cubic structure can undoubtedly be at least partially attributed to the stabilizing influence of  $M\text{—O}$   $\pi$ -bonding.

Even the simplest model would not predict that  $\pi$ -bonding stabilization of the cubic structure will be the same for all transition metal perovskites. The energy, spatial extent and filling of the  $d$ -orbitals on the octahedral ion all play a role in determining the  $M\text{—O}$   $\pi$ -bonding strength. Furthermore, the  $\sigma$ -bonding orbitals on the  $A$  cation and the  $\pi$ -bonding orbitals on the  $M$  cation are in direct competition for the same orbitals on oxygen (Goodenough, 1971; Choy, Park, Hong & Kim, 1994; Takano *et al.*, 1991). Including the changes in ionic lattice energy that accompany octahedral tilting distortions and a theoretical determination of the lowest energy structure becomes quite complicated. Nevertheless, the fact that all these forces are in competition to determine the structure also provides an excellent opportunity to compare their relative strengths. However, before such a comparison can be made the factors influencing  $M\text{—O}$   $\pi$ -bonding must be better understood.

Table 7. All structurally well characterized  $AMO_3$  perovskites, where  $M$  is a transition metal and the tolerance factor is greater than 0.98

Compound	Tilt system	Tolerance factor	No. of $e$ in $t_{2g}$ orbital	Total no. of $d$ $e^-$	$d$ -Orbital radii*
BaMoO <sub>3</sub>	$a^0a^0a^0$	1.047	2	2	0.49
BaNbO <sub>3</sub>	$a^0a^0a^0$	1.031	1	1	0.51
SrVO <sub>3</sub>	$a^0a^0a^0$	1.022	1	1	0.26
SrFeO <sub>3</sub>	$a^0a^0a^0$	1.020	3	4	0.22
BaZrO <sub>3</sub>	$a^0a^0a^0$	1.011	0	0	0.54
SrTiO <sub>3</sub>	$a^0a^0a^0$	1.009	0	0	0.28
SrRuO <sub>3</sub>	$a^+b^-b^-$	1.001	4	4	0.45
SrMoO <sub>3</sub>	$a^0a^0a^0$	0.986	2	2	0.49
CaMnO <sub>3</sub>	$a^+b^-b^-$	1.012	3	3	0.23
CaVO <sub>3</sub>	$a^+b^-b^-$	0.986	1	1	0.26
CaTiO <sub>3</sub>	$a^+b^-b^-$	0.973	0	0	0.28
LaCuO <sub>3</sub>	$a^-a^-a^-$	1.013	6	8	0.185
LaCoO <sub>3</sub>	$a^-a^-a^-$	1.011	6†	6	0.21
LaNiO <sub>3</sub>	$a^-a^-a^-$	1.003	6	7	0.195
PrCoO <sub>3</sub>	$a^-a^-a^-$	0.989	6	6	0.21
PrNiO <sub>3</sub>	$a^-b^-b^-$	0.981	6	7	0.195

\* The radii of the  $d$ -orbitals are theoretical pseudopotential radii and are in atomic units (Zunger, 1980). † In LaCoO<sub>3</sub> the Co<sup>3+</sup> is intermediate between high and low spin and therefore the number of  $t_{2g}$  electrons is not well defined.

Extended Hückel calculations were performed on an  $a^0a^0a^0$  cubic SrMO<sub>3</sub> structure and an  $a^+b^-b^-$  SrMO<sub>3</sub> structure. The  $M$ —O bond distance was 1.98 Å in both structures and the tilt angles in the orthorhombic system were  $-5.9$ ,  $6.1$  and  $6.1^\circ$ . The calculations were carried out for both structures using the EHTB parameters of Mo for the  $M$ -site cation and repeated using the EHTB parameters of Ru. The calculations were performed with Sr on the A site and repeated for a  $MO_3^{2-}$  lattice. In each calculation the number of valence electrons was varied to simulate the presence of 0–6 electrons in the  $4d$ -orbitals of the  $M$  cation. The structures and atomic parameters used in these calculations were chosen to most closely approximate the actual structures of SrMoO<sub>3</sub> and SrRuO<sub>3</sub>. These two compounds were chosen for analysis because even though SrMoO<sub>3</sub> has a smaller tolerance factor than SrRuO<sub>3</sub>, the former compound is cubic while the latter is orthorhombic. Therefore, the energetic changes associated with  $M$ —O  $\pi$ -bonding across the  $4d$ -series appear to be the structure-determining forces in these compounds.

Fig. 6 shows graphically the results of these calculations. It is encouraging that the calculations predict that SrMoO<sub>3</sub> will be cubic and SrRuO<sub>3</sub> will be orthorhombic. However, the trends apparent in Fig. 6 are more important than the absolute energy differences between structures, which are quite small. Three generalizations can be drawn from these calculations. First, the  $M$ —O  $\pi$ -bonding stabilization of the cubic structure is largest for  $d^1$ - and  $d^2$ -octahedral cations and decreases as the  $\pi^*$ -band becomes increasingly populated. Secondly, the presence of Sr stabilizes the orthorhombic structure with respect to the cubic structure, even though Sr—O oxygen

bonds show only a small degree of covalency. Finally, substitution of the more electronegative Ru, for Mo, stabilizes the orthorhombic structure, particularly in the presence of Sr or when the  $\pi^*$ -band is almost full.

The results in Fig. 6 can be understood in the following way. The immediate environment about the  $M$  cations, which is primarily responsible for determining the  $\pi$ - and  $\pi^*$ -energy levels, is the same for both the cubic and orthorhombic structures. On the other hand, the orbital overlap across  $M$ —O— $M$  linkages, which allows electron delocalization, is better in the cubic structure. The former interaction, to a first approximation, dictates the position of the center of the  $\pi^*$ -band, whereas the latter interaction determines the width of the  $\pi^*$ -band. This leads to an orthorhombic  $\pi^*$ -band which is more narrow than the cubic  $\pi^*$ -band, but centered at approximately the same energy. Fig. 7 depicts an exaggerated density-of-states band picture that corresponds to this situation. As the  $\pi^*$ -band begins to fill the total energy of the cubic structure will be lower than the orthorhombic structure. This is because the bottom of the cubic  $\pi^*$ -band is at a lower energy than the bottom of the orthorhombic  $\pi^*$ -band. If the two bands are centered at exactly the same energy, the maximum stabilization of the cubic structure will occur when the  $\pi^*$ -band is half filled, corresponding to a  $d^3$ -octahedral cation. As the  $\pi^*$ -band continues to fill the energy stabilization of the cubic structure will begin to decrease, until the band is completely filled and the two structures once again have the same energy. If the center of the narrow band is at a slightly lower energy than the center of the broad band, the maximum stabilization will be shifted from a half-filled band to a somewhat lesser degree of filling and the total energy

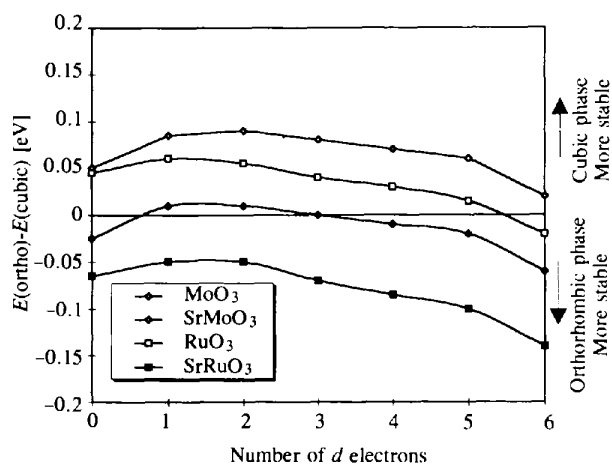


Fig. 6. The energy difference as calculated by the EHTB method between the cubic ( $a^0a^0a^0$  tilt system) and the orthorhombic ( $a^+b^-b^-$  tilt system) structures for SrMO<sub>3</sub> compounds. The open diamonds represent calculations on a MoO<sub>3</sub><sup>2-</sup> lattice, the filled diamonds a SrMoO<sub>3</sub> lattice, the open squares a RuO<sub>3</sub><sup>2-</sup> lattice and the filled squares a SrRuO<sub>3</sub> lattice.

of the completely filled narrow band will be lower than the total energy of the completely filled broad band. Both these trends are observed in Fig. 6, indicating that the energy center of the orthorhombic  $\pi^*$ -band has a slightly lower energy than the energy center of the cubic  $\pi^*$ -band. The band centers are not at exactly the same energy, because the oxygen cannot form perfect overlaps with both metal cations in the orthorhombic structure. This reduces the antibonding character of the  $\pi^*$ -band (increases its nonbonding character), thus lowering its energy somewhat.

The effect of substituting ruthenium for molybdenum can also be explained in a straightforward manner. It is directly related to the fact that ruthenium is more electronegative than molybdenum and the Ru  $4d$ -orbitals will therefore be lower in energy than the Mo  $4d$ -orbitals. To understand the effect of this change, consider the interaction between a metal orbital and a lower energy oxygen orbital to form a bonding orbital and an antibonding orbital, as depicted in Fig. 8. If the metal orbital is lowered in energy, by the amount  $E_m$ , then the energy overlap of the two levels is improved. This results in a small increase in the stabilization of the bonding orbital and a destabilization of the antibonding orbital. If the interaction is somehow changed so that no bonding interaction occurs and only two nonbonding levels exist, the only change will be a lowering of the upper level. Therefore, the energy difference between the antibonding and nonbonding levels,  $\Delta E_1$  and  $\Delta E_2$ , will increase as the energy separation between the metal and oxygen energy levels decreases, due to the increased destabilization of the antibonding orbital. In other words, the relationship  $\Delta E_1 < \Delta E_2$  will always hold. This analysis can be applied to the perovskite structure in the following way. Since the spatial overlap of orbitals is reduced in the orthorhombic structure, the  $\pi^*$ -band has a larger metal  $t_{2g}$ -nonbonding component than the same band in the cubic structure. Therefore, lowering the energy of the  $4d$ -orbitals in SrRuO<sub>3</sub> causes the center of the  $\pi^*$ -band in the cubic structure to shift

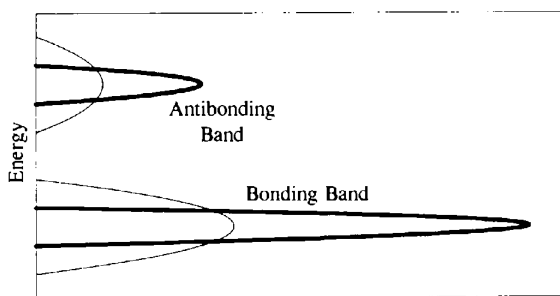


Fig. 7. An exaggerated representation of the density of electronic states associated with the  $\pi$  (bonding) and  $\pi^*$  (antibonding) bands in a perovskite. The thick line represents a poor  $M-O-M$  overlap which results in narrow bands. The fine line represents a good  $M-O-M$  overlap and broader bands.

upwards relative to the center of the same band in the orthorhombic structure. This will result in a stabilization of the orthorhombic structure, relative to the cubic structure, especially as the  $\pi^*$ -band becomes increasingly populated.

The prediction that the presence of Sr stabilizes the orthorhombic structure is consistent with the earlier analysis of covalent  $A-O$  interactions, which showed that covalent  $A-O$  bonding was optimized in the orthorhombic  $a^+b^-b^-$  tilt system. However, these calculations contain two additional points of interest. First, in the case of SrRuO<sub>3</sub> the calculations only predict the orthorhombic structure to be more stable when Sr is included in the calculation. Second, the electronegativity of strontium is much smaller than that of yttrium and Sr—O bonds have only a small degree of covalency. Yet the calculations suggest that even this weak covalent interaction is sufficient to stabilize the distorted structure over the cubic structure. Since the  $A$  cation  $\sigma$ -bonding orbitals and  $M$  cation  $\pi$ -bonding orbitals both overlap with the same orbitals on oxygen, the formation of covalent  $A-O$  bonds will reduce the electron density in the  $M-O$   $\pi$ - and  $\pi^*$ -bonds. Presumably, this will originate primarily from the higher energy  $\pi^*$ -band. In this way, formation of  $A-O$  bonds may actually strengthen the  $M-O$  bonds. This effect should be most evident in the orthorhombic  $a^+b^-b^-$  structure, which has already been shown to maximize the  $A-O$  covalent interactions. This might explain why the orthorhombic structure is favored over the rhombohedral structure. Of course, the Madelung energy contribution also favors the orthorhombic and rhombohedral structures over the cubic structure. Another possibility, if the ionic

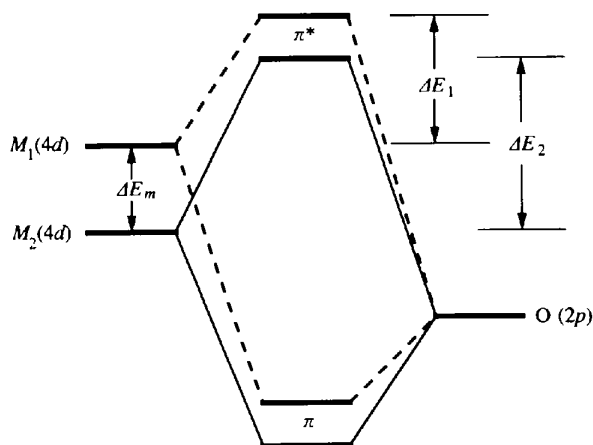


Fig. 8. A schematic representation of the effect that lowering the energy of the metal orbital, in a  $M(4d)-O(2p)$  interaction, has on the bonding and antibonding levels. The energy  $E_1$  is the difference in energy between the antibonding level and the nonbonding level before lowering the energy of the metal  $4d$ -orbital. The energy  $E_2$  is the same energy difference after lowering the energy of the metal  $4d$ -orbital, by  $E_m$ .

contribution to the total energy is dominant, is that the Sr—O repulsion is large enough (the tolerance factor is greater than 1, yet the structure is distorted) to destabilize the rhombohedral structure with respect to the orthorhombic structure.

Equipped with a better understanding of  $M$ —O bonding interactions we are now prepared to analyze Table 7. The compounds in Table 7 can be grouped into three categories. The first eight compounds all have either Ba or Sr on the  $A$  site and one of the early  $3d$ - or  $4d$ -transition metals on the  $M$  site. These compounds have all the attributes which stabilize the cubic structure. The  $A$  cations here are quite basic, so that  $A$ —O covalency is expected to be small. The early transition metals have  $t_{2g}$ -orbitals with a fairly large spatial extent, for good overlap with oxygen  $2p$ -orbitals. This is more true of the  $4d$ -transition metals than the  $3d$ -transition metals. Furthermore, all these ions have  $t_{2g}$ -orbitals that are less than half full. The exception is  $\text{SrRuO}_3$ , which is also the only compound of the eight that is not cubic. The forces that cause  $\text{SrRuO}_3$  to be orthorhombic have been discussed in detail above. Due to its intermediate position between  $\text{SrMoO}_3$  and  $\text{SrRuO}_3$  it would be very interesting if  $\text{SrTcO}_3$  could be synthesized and structurally characterized. The next two compounds have Ca on the  $A$  site and a  $3d$ -transition metal on the  $M$  site. Both these compounds are orthorhombic, even though their tolerance factors are in the same range where cubic compounds were observed among the first eight compounds. There are two possible reasons for this change in structure. First, calcium is more electronegative than either barium or strontium, resulting in increased covalency in the  $A$ —O bonds and stabilizing the orthorhombic structure. Second, because of decreased spatial and energetic overlap between oxygen  $2p$ - and metal  $3d$ -orbitals the  $\pi$ -bonding stabilization of the cubic structure will be smaller when  $M$  is a  $3d$ -transition metal than when it is a  $4d$ -transition metal. However, when  $A = \text{Ca}$  and  $M$  is a  $4d$ -transition metal the tolerance factor is always smaller than 0.97, so it is unknown whether  $\pi$ -bonding could be increased to the point where it stabilized the cubic structure, despite the presence of calcium on the  $A$  site. The last five compounds all have one of the larger lanthanide ions on the  $A$  site and one of the later elements from the  $3d$ -transition series on the  $M$  site. Once again this is the only combination, of lanthanides with transition metals, that leads to a tolerance factor larger than 0.98. The attributes of this group of compounds are well suited to the rhombohedral structure. All the transition metals have filled  $t_{2g}$ -shells so that  $\pi$ -bonding stabilization of the cubic structure is negated. Furthermore, the trivalent cation on the  $A$  site maximizes the ionic interaction between the  $A$ -site ion and oxygen. This interaction is optimized in the rhombohedral structure. Finally, the tolerance factor values fall into a range where repulsive forces between the  $A$ -site ion and oxygen

are not large enough to destabilize the rhombohedral structure. Not surprisingly, all these compounds adopt the rhombohedral structure.

### 5. Nonequivalent $A$ -site tilt systems

The tilt systems already discussed account for the majority of the known distorted perovskites. However, when the two  $A$ -site cations become very different, such as an alkaline earth and a transition metal, the tilt systems with nonequivalent  $A$  sites become important. Tilt systems 17,18 ( $0+$ ) and 4-7 ( $++$ ) are similar in that half of the  $A$ -cation sites become suitable for small cations, while the other half remain suitable for large  $A$  cations. The large cation site is described in Table 1 as face-centered trigonal prismatic. This description is meant to describe the coordination that would result if the  $A$  cation was moved from the center of a trigonal prism toward one of the rectangular faces. As with the eight-coordinate site in the  $a^+b^-b^-$  system, the distribution of bond distances is probably more important than the exact coordination geometry. The small  $A$ -cation sites in these systems are distorted tetrahedral sites in tilt systems 17 and 18, and a 50:50 mixture of distorted tetrahedral and square-planar sites in tilt systems 4-7. Excluding high-temperature phases, the only compound known to adopt one of these six tilt systems is  $\text{CaFeTi}_2\text{O}_6$  (Leinenweber & Parise, 1995). This compound has the expected distribution of cations with  $\text{Ca}^{2+}$  occupying the large  $A$ -cation sites and  $\text{Fe}^{2+}$  occupying the smaller tetrahedral and square-planar sites. Tilt systems 15,16 ( $0++$ ) have a different distribution of  $A$ -cation sites. In  $a^0b^+b^+$  one half of the  $A$  sites are very similar to the  $A$ -site coordination found in  $a^0a^0c^+$ , one quarter of the  $A$  sites are in a highly symmetrical eight-coordinate cubic coordination and the remaining  $A$  sites are square planar with a considerably smaller coordination sphere. Thus, 75% of the  $A$ -cation sites can accommodate large  $A$  cations and the other 25% are only suitable for smaller  $A$  cations.

The  $a^+a^+a^+$  tilt system is interesting in part, because even though it can be highly distorted from the ideal perovskite structure it is cubic ( $Im\bar{3}$ ). In this structure 25% of the  $A$ -cation sites are coordinated by 12 equidistant anions in a geometry only slightly displaced from the cubo-octahedral geometry found in the undistorted perovskite structure. The remaining  $A$ -cation sites have a considerably smaller first coordination sphere that is perfectly square planar. The  $a^+b^+c^+$  (1) and  $a^+b^+b^+$  (2) tilt systems have similar  $A$ -cation site distributions. Of these five tilt systems (1, 2, 3, 15 and 16) actual compounds are only observed for tilt system 3,  $a^+a^+a^+$  (see Table 2). Many of the compounds found in this space group, including  $\text{CaFe}_3\text{Ti}_4\text{O}_{12}$  (Leinenweber & Parise, 1995),  $\text{CaCu}_3\text{Ge}_4\text{O}_{12}$  (Ozaki, Ghedira, Chenevas, Joubert & Marezio, 1977),  $\text{CaCu}_3\text{Mn}_4\text{O}_{12}$  (Chenevas, Joubert, Marezio & Bochu, 1975) and  $\text{NaMn}_3\text{Mn}_4\text{O}_{12}$  (Marezio, Dernier, Chenevas & Joubert, 1973), were

synthesized under high pressure where  $\frac{3}{4}$  of the *A* cations are smaller transition metals (Fe and Mn) and  $\frac{1}{4}$  of the *A* cations are larger alkali, alkaline earth or rare earth metals. In this structure the transition metals occupy the square-planar site, while the larger cations occupy the 12-coordinate site. Some of the compounds belonging to this tilt system were synthesized in air at ambient pressure, such as the ruthenates (Labeau, Bochu, Joubert & Chenevas, 1980) and titanates (Bochu *et al.*, 1979) in Table 2. All these compounds have the Jahn–Teller ion  $\text{Cu}^{2+}$  on the square-planar *A*-cation sites. The  $\text{Cu}^{2+}$  ion occupies the square-planar sites in preference to the octahedral sites, thus lifting the degeneracy of the copper-based  $e_g$ -orbitals. The list of  $a^+a^+a^+$  compounds in Table 2 is not exhaustive, but not surprisingly all compounds omitted from Table 2 have a Jahn–Teller transition metal cation, such as  $\text{Cu}^{2+}$  or  $\text{Mn}^{3+}$ , on  $\frac{3}{4}$  of the *A*-cation sites. In general, this tilt system should be quite stable whenever  $\frac{3}{4}$  of the *A*-cation sites are filled with cations that prefer square-planar coordination and the other  $\frac{1}{4}$  of the *A*-cation sites are filled by larger cations compatible with a cubo-octahedral coordination.

The information contained in Tables 1 and 2 for tilt systems with nonequivalent *A* sites suggests that it is possible that many more of these compounds could be synthesized with the proper choice and ratio of ions. It seems reasonable to assume that the tilt system achieved will be directly dependent upon the ratio of large,  $A_L$ , to small cations,  $A_S$ , on the *A* site. When the  $A_L/A_S$  ratio is 3:1 tilt systems 15 and 16 (0++) should be favored, when the  $A_L/A_S$  ratio is 1:1 tilt systems 17 and 18 (0+-) or 4-7 (++) should be favored and when  $A_L/A_S$  is 1:3 tilt systems 1-3 (+++) should be favored. Of course, in order to move the small cations onto the *A* site high-pressure synthesis may be necessary. In such a synthetic search *POTATO* could prove useful for predicting which combination of ions will have the proper size match to form a stable compound.

## 6. Conclusions

The various tilt systems have been compared in terms of their *A*-cation coordination and it has been shown that the tilt systems where all of the *A*-cation sites remain crystallographically equivalent are strongly favored when there is a single ion on the *A* site. Of these tilt systems the orthorhombic  $a^+b^-b^-$  tilt system has been shown to maximize *A*–O covalent bonding and minimize repulsive *A*–O overlap. For these reasons the orthorhombic  $\text{GdFeO}_3$  structure is found almost exclusively when the tolerance factor becomes smaller than 0.975 or when the *A*-site cation becomes relatively electronegative, as is the case when *A* = Ca. Madelung energy calculations show the undistorted cubic  $a^0a^0a^0$  tilt to be unstable with respect to distorted tilt systems. This structure is stabilized only by ion–ion repulsion in the case of oversized *A* cations and *M*–O  $\pi$ -

Table 8. *Extended Hückel parameters*

Atom	<i>d</i>	$H_{ii}$ (eV)			Orbital exponent $\zeta$		
		<i>s</i>	<i>p</i>	<i>d</i> *	<i>s</i>	<i>p</i>	
O		-32.30	-14.80		2.28	2.28	
Al		-12.30	-6.50		1.37	1.36	
Sr		-6.62	-3.92		1.21	1.21	
Y	-8.32	-8.13	-5.14	1.56 (0.8316) 3.55 (0.3041)	1.74	1.70	
Mo	-11.06	-8.77	-5.60	4.54 (0.5899) 1.90 (0.5899)	1.96	1.90	
Ru	-14.62	-10.79	-5.74	5.38 (0.5573) 2.30 (0.6642)	2.08	2.04	
Sn		-16.16	-8.32		2.12	1.82	

\*The *d*-orbitals are modeled using a double  $\zeta$  expansion. For a description of the use of these parameters in the extended Hückel method see Burdett (1980).

bonding interactions when *M* is an early transition metal cation. The rhombohedral  $a^-a^-a^-$  tilt system is most commonly observed in those cases where the tolerance factor is in the range 0.975–1.02 and the ionic charge on the *A*-site cation is large. These factors favor the rhombohedral structure because it maximizes the *A*–O ionic interaction and keeps the ion–ion repulsion from becoming too large. Tilt systems with nonequivalent *A*-site environments will be favored in compounds where at least two *A* cations with different sizes and/or bonding preferences are present. The ratio of large to small cations will dictate the most stable tilt system.

I would like to thank Dong-Kyun Seo for many helpful comments on the use and interpretation of the extended Hückel method. I would also like to thank Dr Arthur Sleight for his support and many helpful suggestions throughout this project. Finally, I owe a deep debt of gratitude to Dr John Evans for countless discussions and helpful comments over the entire period of this work and particularly for his help with the *GULP* calculations. Without the advice and support of these individuals this work would not have been possible.

## APPENDIX A

The atomic parameters used in the extended Hückel calculations were provided by the software package used in the calculations (Miller, 1990). They are given in Table 8.

## References

- Abrahams, S. C. & Bernstein, J. L. (1967). *J. Phys. Chem. Solids*, **28**, 1685–1692.
- Ahtee, M. & Darlington, C. N. W. (1980). *Acta Cryst.* **B36**, 1007–1014.
- Ahtee, A., Ahtee, M., Glazer, A. M. & Hewat, A. W. (1976). *Acta Cryst.* **B32**, 3243–3246.
- Ahtee, M., Glazer, A. M. & Hewat, A. W. (1978). *Acta Cryst.* **B34**, 752–758.

- Ahtee, M., Glazer, A. M. & Megaw, H. (1972). *Philos. Mag.* **26**, 995–1014.
- Aleksandrov, K. S. (1976). *Kristallografiya*, **21**, 249–255.
- Alter, E. (1974). *Z. Anorg. Allg. Chem.* **408**, 115–120.
- Bartram, S. F. & Fryxell, R. E. (1970). *J. Inorg. Nucl. Chem.* **32**, 3701–3706.
- Battle, P. D., Gibb, T. C. & Lightfoot, P. (1990). *J. Solid State Chem.* **84**, 271–279.
- Benner, G. & Hoppe, R. (1990). *J. Fluorine Chem.* **46**, 283–295.
- Bensch, W., Schmalte, H. W. & Reller, A. (1990). *Solid State Ion.* **43**, 171–177.
- Bidaux, R. & Mériel, P. (1968). *J. Phys. Radium*, **29**, 220–224.
- Blasse, G. (1965). *J. Inorg. Nucl. Chem.* **27**, 993–1003.
- Bochu, B., Deschizeaux, N. N., Joubert, J. C., Collomb, A., Chenevas, J. & Marezio, M. (1979). *J. Solid State Chem.* **29**, 291–298.
- Bouloux, J.-C. & Galy, J. (1976). *J. Solid State Chem.* **16**, 385–391.
- Brese, N. E. & O'Keeffe, M. (1991). *Acta Cryst.* **B47**, 192–197.
- Brixner, L. H. (1960). *J. Inorg. Nucl. Chem.* **14**, 225–230.
- Brochu, R., Padiou, J. & Grandjean, D. (1970). *C. R. Acad. Sci. Ser. C*, **271**, 642–643.
- Brown, I. D. (1981). *Structure and Bonding in Crystals*, edited by M. O'Keeffe & A. Navrotsky, Vol. 2, pp. 1–30. New York: Academic Press.
- Brynstad, J., Yakel, H. L. & Smith, G. P. (1966). *J. Chem. Phys.* **45**, 4652–4664.
- Burbank, R. D. (1970). *J. Appl. Cryst.* **3**, 112–120.
- Burdett, J. K. (1980). *Molecular Shapes*, Ch. 2. New York: John Wiley & Sons.
- Burdett, J. K. & Mitchell, J. F. (1993). *Chem. Mater.* **5**, 1465–1473.
- Bush, T. S., Catlow, C. R. A., Chadwick, A. V., Cole, M., Geatches, R. M., Greaves, G. N. & Tomlinson, S. M. (1992). *J. Mater. Chem.* **2**, 309–316.
- Bush, T. S., Gale, J. D., Catlow, R. A. & Battle, P. D. (1994). *J. Mater. Chem.* **4**, 831–837.
- Buttner, R. H. & Maslen, E. N. (1988). *Acta Cryst.* **C44**, 1707–1709.
- Chenevas, J., Joubert, J. C., Marezio, M. & Bochu, B. (1975). *J. Solid State Chem.* **14**, 25–32.
- Choy, J.-H., Park, J. H., Hong, S.-T. & Kim, D. K. (1994). *J. Solid State Chem.* **111**, 370–379.
- Christoph, C. G., Larson, A. C., Eller, P. G., Purson, J. D., Zahrt, J. D., Penneman, R. A. & Rinehart, G. H. (1988). *Acta Cryst.* **B44**, 575–580.
- Clearfield, A. (1963). *Acta Cryst.* **16**, 135–142.
- Collomb, A., Samaras, D., Buevoz, J. L., Levy, J. P. & Joubert, J. C. (1983). *J. Magn. Magn. Mater.* **40**, 75–82.
- Dann, S. E., Currie, D. B., Weller, M. T., Thomas, M. F. & Al Rawwas, A. D. (1994). *J. Solid State Chem.* **109**, 134–144.
- Darlington, C. N. W. (1971). Thesis. University of Cambridge.
- Deblieck, R., Van Tendeloo, G., Van Landuyt, J. & Amelinckx, S. (1985). *Acta Cryst.* **B41**, 319–329.
- Demazeau, G., Parent, C., Pouchard, M. & Hagenmueller, P. (1972). *Mater. Res. Bull.* **7**, 913–920.
- Derighetti, B., Drumheller, J. E., Laves, F., Müller, K. A. & Waldner, F. (1965). *Acta Cryst.* **18**, 557.
- Deschizeaux, M. N., Joubert, J. C., Vegas, A., Collomb, A., Chenevas, J. & Marezio, M. (1976). *J. Solid State Chem.* **19**, 45–51.
- Dickens, P. G. & Powell, A. V. (1991). *J. Mater. Chem.* **1**, 137–138.
- Diehl, R. & Brandt, G. (1975). *Mater. Res. Bull.* **10**, 85–90.
- Diehl, R., Brandt, G. & Salje, E. (1978). *Acta Cryst.* **B34**, 1105–1111.
- Elemans, J. B. A., van Laar, B., van der Veen, K. R. & Loopstra, B. O. (1971). *J. Solid State Chem.* **3**, 238–242.
- Ferretti, A., Rogers, D. B. & Goodenough, J. B. (1965). *J. Phys. Chem. Solids*, **26**, 2007–2011.
- Fesenko, E. G., Razumovskaya, O. N., Shuvaeva, V. A., Gridneva, G. G. & Bunina, O. A. (1991). *Isv. Akad. Nauk SSSR Neorg. Mater.* **27**, 1991–1992.
- Flocken, J. W., Guenther, R. A., Hardy, J. R. & Boyer, L. L. (1985). *Phys. Rev. B*, **31**, 7252–7255.
- Flocken, J. W., Guenther, R. A., Hardy, J. R. & Boyer, L. L. (1986). *Phys. Rev. Lett.* **56**, 1738–1741.
- Forquet, J. E., Renou, M. F., De Pape, R., Theveneau, H., Man, P. P., Lucas, O. & Pannetier, J. (1983). *Solid State Ion.* **9**, 1011–1014.
- Galasso, F. S. (1969). *Structure, Properties, and Preparation of Perovskite Type Compounds*. Oxford: Pergamon Press.
- Gale, J. D. (1992/1994). *GULP. General Utility Lattice Program*. Royal Institution and Imperial College, London.
- García-Muñoz, J. L., Rodríguez-Carvajal, J., Lacorre, P. & Torrance, J. B. (1992). *Phys. Rev. B*, **46**, 4414–4425.
- Geller, S. & Wood, E. A. (1956). *Acta Cryst.* **9**, 563–568.
- Glazer, A. M. (1972). *Acta Cryst.* **B28**, 3384–3392.
- Glazer, A. M. & Megaw, H. (1972). *Philos. Mag.* **25**, 1119–1135.
- Goldschmidt, V. M. (1926). *Naturwissenschaften*, **14**, 477–485.
- Goodenough, J. B. (1963). *Magnetism and the Chemical Bond*. New York: Wiley Interscience.
- Goodenough, J. B. (1967). *Phys. Rev.* **164**, 785–789.
- Goodenough, J. B. (1971). *Prog. Solid State Chem.* **5**, 145–391.
- Goodenough, J. B. & Kafalas, J. A. (1972). *J. Solid State Chem.* **6**, 493–501.
- Greedan, J. E., Willmer, K. L. & Gibbs, H. F. (1992). *Eur. J. Solid State Chem.* **29**, 505–518.
- Hägg, G. (1935). *Z. Phys. Chem. Abt. B*, **29**, 192–196.
- Hemley, R. J., Cohen, R. E., Yeganeh-Haeri, A., Mao, H. K., Weidner, D. J. & Ito, E. (1989). *Geophysical Monographs (Perovskite – A Structure of Great Interest to Geophysics and Materials Science)*, edited by A. Navrotsky & D. Weidner, Vol. 45, pp. 35–44. Washington DC: American Geophysical Union.
- Hepworth, M. A., Jack, K. H., Peacock, R. D. & Westland, G. J. (1957). *Acta Cryst.* **10**, 63–69.
- Hoffmann, R. (1963). *J. Chem. Phys.* **39**, 1397–1412.
- Hoffmann, R. (1988). *Solids and Surfaces: A Chemist's View of Bonding in Extended Structures*. New York: VCH Publishers.
- Hohnstedt, C. & Meyer, G. (1993). *Z. Anorg. Allg. Chem.* **619**, 1374–1378.
- Hönle, W. & Simon, A. (1986). *Z. Naturforsch. Teil B*, **41**, 1391–1398.
- Hönle, W., Miller, G. & Simon, A. (1988). *J. Solid State Chem.* **75**, 147–155.
- Horowitz, A., Amit, M., Makovsky, J., Ben Dör, L. & Kalman, Z. H. (1982). *J. Solid State Chem.* **43**, 107–125.
- Huang, T. C., Parrish, W., Toraya, H., Lacorre, P. & Torrance, J. B. (1990). *Mater. Res. Bull.* **25**, 1091–1098.

- Hyde, B. G. & Andersson, S. (1988). *Inorganic Crystal Structures*, Ch. XI. New York: Wiley Interscience.
- Jacobson, A. J., Tofield, B. C. & Fender, B. E. F. (1972). *Acta Cryst.* **B28**, 956–961.
- Jirak, Z., Pollert, E., Andersen, A. F., Grenier, J.-C. & Hagenmuller, P. (1990). *Eur. J. Solid State Inorg. Chem.* **27**, 421–433.
- Jones, C. W., Battle, P. D., Lightfoot, P. & Harrison, W. T. A. (1989). *Acta Cryst.* **C45**, 365–367.
- Kamata, K., Nakamura, T. & Sata, T. (1975). *Chem. Lett.* **1**, 81–86.
- Keller, H. L., Meier, K. H. & Müller-Buschbaum, H. (1975). *Z. Naturforsch.* **30**, 277–278.
- Khattak, C. P. & Cox, D. E. (1977). *Mater. Res. Bull.* **12**, 463–472.
- Kijima, N., Tanaka, K. & Marumo, F. (1981). *Acta Cryst.* **B37**, 545–548.
- Kijima, N., Tanaka, K. & Marumo, F. (1983). *Acta Cryst.* **B39**, 557–561.
- Kohn, K., Inoue, K., Horie, O. & Akimoto, S.-I. (1976). *J. Solid State Chem.* **18**, 27–37.
- Koopmanns, H. J. A., van de Velde, G. M. H. & Gellings, P. J. (1983). *Acta Cryst.* **C39**, 1323–1325.
- Labeau, M., Bochu, B., Joubert, J. C. & Chenevas, J. (1980). *J. Solid State Chem.* **33**, 257–261.
- Lacorre, P., Torrance, J. B., Pannetier, J., Nazzari, A. I., Wang, P. W. & Huang, T. C. (1991). *J. Solid State Chem.* **91**, 225–237.
- Leinenweber, K. & Parise, J. (1995). *J. Solid State Chem.* **114**, 277–281.
- Liu, G., Zhao, X. & Eick, H. A. (1992). *J. Alloys Compd.* **187**, 145–156.
- Loopstra, B. O. & Rietveld, H. M. (1969). *Acta Cryst.* **B25**, 1420–1421.
- Luetger, B. & Babel, D. (1992). *Z. Anorg. Allg. Chem.* **616**, 133–140.
- MacLean, D. A., Ng, H.-K. & Greedan, J. E. (1979). *J. Solid State Chem.* **30**, 35–44.
- Mackrodt, W. C. (1984). *Solid State Ion.* **12**, 175–188.
- Marezio, M., Dernier, P. D., Chenevas, J. & Joubert, J. C. (1973). *J. Solid State Chem.* **6**, 16–20.
- Marezio, M., Dernier, P. D. & Remeika, J. P. (1972). *J. Solid State Chem.* **4**, 11–19.
- Marezio, M., Remeika, J. P. & Dernier, P. D. (1970). *Acta Cryst.* **B26**, 2008–2022.
- Marx, D. T., Radaelli, P. G., Jorgensen, J. D., Hitterman, R. L., Hinks, D. G., Pei, S. & Dabrowski, B. (1992). *J. Phys. B Condens. Matter*, **46**, 1144–1156.
- Megaw, H. D. (1968). *Acta Cryst.* **A24**, 583–588.
- Megaw, H. D. & Darlington, C. N. W. (1975). *Acta Cryst.* **A31**, 161–173.
- Michel, C., Moreau, J.-M., Achenbach, G., Gerson, R. & James, W. J. (1969). *Solid State Commun.* **7**, 701–704.
- Miller, G. (1990). *NEW5. Extended Hückel Band Structure Calculation Program*. Iowa State University.
- Minkiewicz, V. J., Fujii, Y. & Yamada, Y. (1970). *J. Phys. Soc. Jpn.* **28**, 443–450.
- Miyata, N., Tanaka, K. & Marumo, F. (1983). *Acta Cryst.* **B39**, 561–564.
- Morin, F. J. (1961). *J. Appl. Phys.* **32**, 2195–2202.
- Müller, J., Haouzi, A., Laviron, C., Labeau, M. & Joubert, J. C. (1986). *Mater. Res. Bull.* **21**, 1131–1136.
- Navrotsky, A. (1989). *Geophysical Monographs (Perovskite – A Structure of Great Interest to Geophysics and Materials Science)*, edited by A. Navrotsky & D. Weidner, Vol. 45, pp. 67–69. Washington DC: American Geophysical Union.
- Noël, H., Padiou, J. & Prigent, J. (1975). *C. R. Acad. Sci. Ser. C*, **280**, 123–126.
- Odenthal, R. H. & Hoppe, R. (1971). *Monatsh. Chem.* **102**, 1340–1350.
- O’Keeffe, M. (1989). *Struct. Bonding (Berlin)*, **71**, 162–190.
- O’Keeffe, M. (1992). *Eutax. Program for Calculating Bond Valences*. EMLab Software, Phoenix, Arizona, USA.
- O’Keeffe, M. & Hyde, B. G. (1977). *Acta Cryst.* **B33**, 3802–3813.
- Ozaki, Y., Ghedira, M., Chenevas, J., Joubert, J. C. & Marezio, M. (1977). *Acta Cryst.* **B33**, 3615–3617.
- Parise, J. B., McCarron III, E. U. & Sleight, A. W. (1987). *Mater. Res. Bull.* **22**, 803–811.
- Pauling, L. (1929). *J. Am. Chem. Soc.* **51**, 1010–1026.
- Poepelmeier, K. R., Leonowicz, M. E., Scanlon, J. C., Longo, J. M. & Yelon, W. B. (1982). *J. Solid State Chem.* **45**, 71–79.
- Quezel-Ambrunaz, S. (1968). *Bull. Soc. Fr. Minér. Cristallogr.* **91**, 339–343.
- Randall, C. A., Bhalla, A. S., Shrout, T. R. & Cross, L. E. (1990). *J. Mater. Res.* **5**, 829–834.
- Rango, C. de, Tsoucaris, G. & Zelwer, C. (1966). *Acta Cryst.* **20**, 590–592.
- Rey, M. J., Dehault, P. H., Joubert, J. C., Lambert-Andron, B., Cyrot, M. & Cyrot-Lackmann, F. (1990). *J. Solid State Chem.* **86**, 101–108.
- Ritter, H., Ihringer, J., Maichle, J. K., Prandl, W., Hoser, A. & Hewat, A. W. (1989). *Z. Phys. B*, **75**, 297–302.
- Rodier, N. & Laruelle, P. (1970). *C. R. Acad. Sci.* **270**, 2127–2130.
- Rodier, N., Julien, R. & Tien, V. (1983). *Acta Cryst.* **C39**, 670–673.
- Roth, R. S. (1957). *J. Res. Natl Bur. Stand.* **58**, 75–88.
- Saiki, A., Seto, Y., Seki, H., Ishizawa, N., Kato, M. & Mizutani, N. (1991). *J. Chem. Soc. Jpn.* **1**, 25–31.
- Salje, E. (1977). *Acta Cryst.* **B33**, 574–577.
- Sasaki, S., Prewitt, C. T., Bass, J. D. & Schulze, W. A. (1987). *Acta Cryst.* **C43**, 1668–1674.
- Sasaki, S., Prewitt, C. T. & Liebermann, R. C. (1983). *Am. Mineral.* **68**, 1189–1198.
- Sato, M., Jin, T., Hama, Y. & Uematsu, K. (1993). *J. Mater. Chem.* **3**, 325–326.
- Shannon, R. D. (1976). *Acta Cryst.* **A32**, 751–767.
- Shimizu, Y., Syono, Y. & Akimoto, S. (1970). *High Temp. High Press.* **2**, 113–120.
- Sleight, A. W. & Prewitt, C. T. (1973). *J. Solid State Chem.* **6**, 509–512.
- Smith, A. J. & Welch, A. J. E. (1960). *Acta Cryst.* **13**, 653–659.
- Svensson, C. & Stahl, K. (1988). *J. Solid State Chem.* **77**, 112–116.
- Svensson, G. & Werner, P.-E. (1990). *Mater. Res. Bull.* **25**, 9–14.
- Takano, M., Nasu, S., Abe, T., Yamamoto, K., Endo, S., Takeda, Y. & Goodenough, J. B. (1991). *Phys. Rev. Lett.* **67**, 3267–3270.

- Takano, M., Okita, T., Nakayama, N., Bando, Y., Takeda, Y., Yamamoto, O. & Goodenough, J. B. (1988). *J. Solid State Chem.* **73**, 140–150.
- Thomas, N. W. (1996). *Acta Cryst.* **B52**, 16–31.
- Thomas, N. W. & Beitollahi, A. (1994). *Acta Cryst.* **B50**, 549–560.
- Thornton, G. & Jacobson, A. J. (1976). *Mater. Res. Bull.* **11**, 837–842.
- Thornton, G., Tofield, B. C. & Hewat, A. W. (1986). *J. Solid State Chem.* **61**, 301–307.
- Tornero, J. D., Cano, F. H., Fayos, J. & Martinez-Ripoll, M. (1978). *Ferroelectrics*, **19**, 123–130.
- Unoki, J. & Sakudo, T. (1967). *J. Phys. Soc. Jpn*, **23**, 546–552.
- Vegas, A., Vallet-Regi, M., Gonzales-Calbet, J. M. & Alario-Franco, M. A. (1986). *Acta Cryst.* **B42**, 167–172.
- Wang, Y., Lu, X., Gao, G. D., Lieberman, R. C. & Dudley, M. (1991). *Mater. Sci. Eng. A*, **132**, 13–21.
- Whangbo, M.-H. & Hoffmann, R. (1978). *J. Am. Chem. Soc.* **100**, 6093–6098.
- Whangbo, M.-H., Evain, M., Canadell, E. & Ganne, M. (1989). *Inorg. Chem.* **28**, 267–271.
- Wiseman, P. J. & Dickens, P. (1973). *J. Solid State Chem.* **3**, 374–380.
- Wiseman, P. J. & Dickens, P. (1976). *J. Solid State Chem.* **17**, 91–100.
- Woodward, P. M. (1997). *J. Appl. Cryst.* Submitted.
- Woodward, P. M., Sleight, A. W. & Vogt, T. (1995). *J. Phys. Chem. Solids*, **56**, 1305–1315.
- Yamada, K., Funabiki, S., Horimoto, H., Matsui, T., Okuda, T. & Ichiba, S. (1991). *Chem. Lett.* pp. 801–804.
- Zhao, C., Feng, S., Zhicheng, C., Shi, C., Xu, R. & Ni, J. (1996). *Chem. Commun.* pp. 1641–1643.
- Zubkov, V. G., Berger, I. F., Pesina, Z. M., Bazuev, G. V. & Shveikin, G. P. (1986). *Sov. Phys. Dokl.* **31**, 459–461.
- Zunger, A. (1980). *Phys. Rev. B*, **23**, 5839–5872.